

Trace Element Partitioning in HP–LT Metamorphic Assemblages during Subduction-related Metamorphism, Ile de Groix, France: a Detailed LA-ICPMS Study

AFIFÉ EL KORH¹*, SUSANNE TH. SCHMIDT¹, ALEXEY ULIANOV² AND SÉBASTIEN POTEL³

¹DEPARTMENT OF MINERALOGY, UNIVERSITY OF GENEVA, RUE DES MARAICHERS 13, CH-1205 GENEVA, SWITZERLAND

²INSTITUTE OF MINERALOGY AND GEOCHEMISTRY, UNIVERSITY OF LAUSANNE, ANTHROPOLE, CH-1015 LAUSANNE, SWITZERLAND

³INSTITUT POLYTECHNIQUE LASALLE BEAUVAIS, 19 RUE PIERRE WAGUET, BP 30313, F-60026 BEAUVAIS, FRANCE

RECEIVED JUNE 30, 2008; ACCEPTED MAY 14, 2009

Devolatilization reactions and subsequent transfer of fluid from subducted oceanic crust into the overlying mantle wedge are important processes, which are responsible for the specific geochemical characteristics of subduction-related metamorphic rocks, as well as those of arc magmatism. To better understand the geochemical fingerprint induced by fluid mobilization during dehydration and rehydration processes related to subduction zone metamorphism, the trace element and rare earth element (REE) distribution patterns in HP–LT metamorphic assemblages in eclogite-, blueschist- and greenschist-facies rocks of the Ile de Groix were obtained by laser ablation inductively coupled plasma mass spectrometry (LA-ICPMS) analysis. This study focuses on 10 massive basic rocks representing former hydrothermally altered mid-ocean ridge basalts (MORB), four banded basic rocks of volcano-sedimentary origin and one micaschist. The main hosts for incompatible trace elements are epidote (REE, Th, U, Pb, Sr), garnet [Y, heavy REE (HREE)], phengite (Cs, Rb, Ba, B), titanite [Ti, Nb, Ta, REE; HREE > LREE (light REE)], rutile (Ti, Nb, Ta) and apatite (REE, Sr). The trace element contents of omphacite, amphibole, albite and chlorite are low. The incompatible trace element contents of minerals are controlled by the stable metamorphic mineral assemblage and directly related to the appearance, disappearance and reappearance of minerals,

especially epidote, garnet, titanite, rutile and phengite, during subduction zone metamorphism. Epidote is a key mineral in the trace element exchange process because of its large stability field, ranging from lower greenschist- to blueschist- and eclogite-facies conditions. Different generations of epidote are generally observed and related to the coexisting phases at different stages of the metamorphic cycle (e.g. lawsonite, garnet, titanite). Epidote thus controls most of the REE budget during the changing P–T conditions along the prograde and retrograde path. Phengite also plays an important role in determining the large ion lithophile element (LILE) budget, as it is stable to high P–T conditions. The breakdown of phengite causes the release of LILE during retrogression. A comparison of trace element abundances in whole-rocks and minerals shows that the HP–LT metamorphic rocks largely retain the geochemical characteristics of their basic, volcano-sedimentary and pelitic protoliths, including a hydrothermal alteration overprint before the subduction process. A large part of the incompatible trace elements remained trapped in the rocks and was recycled within the various metamorphic assemblages stable under changing metamorphic conditions during the subduction process, indicating that devolatilization reactions in massive basic rocks do not necessarily imply significant simultaneous trace element and REE release.

*Corresponding author. Telephone: +0041 22 3796626 or 6624. Fax: +0041 22 3793210. E-mail: Afife.ElKorh@unige.ch

KEY WORDS: *dehydration reactions; epidote; garnet; Ile de Groix; incompatible trace elements; LA-ICPMS; phengite; subduction-related HP–LT metamorphism*

INTRODUCTION

Subduction zones are important sites of crustal recycling and fluid transfer within the Earth, intimately associated with arc magmatism. Physical, petrological and thermal models for the evolution of subduction zones suggest that devolatilization reactions in the downgoing slab can generate large quantities of fluid during the various stages of subduction (e.g. Peacock, 1990, 1993a, 1993b, 2001; Schmidt & Poli, 1998; Bebout *et al.*, 1999; Kerrick & Connolly, 2001; Scambelluri & Philippot, 2001; Rüpke *et al.*, 2004).

Evidence for large-scale hydration of the mantle above subducting slabs comes from blueschist assemblages in serpentinite diapirs observed during Ocean Drilling Program (ODP) 125 in the Marianas forearc (Maekawa, 1993), from the distinctive geochemistry and experimental studies of arc magmas (e.g. Tatsumi *et al.*, 1986; Morris *et al.*, 1990; Schmidt & Poli, 1998), that imply fluid- or melt-mediated transport of slab components into the overlying mantle wedge (e.g. Plank & Langmuir, 1988, 1993), or from double-zone earthquakes that can be related to slab-mantle dehydration reactions (Seno & Gonzalez, 1987; Kirby *et al.*, 1996; Peacock, 2001).

It is generally assumed that hydration of the oceanic lithosphere begins at mid-ocean ridges and is followed by both low- and high-temperature hydrothermal alteration on the ocean floor. In addition, sediments are continuously deposited onto the oceanic crust, adding material containing both pore-water and chemically bound water (Plank & Langmuir, 1998). The transport of these hydrothermally altered metabasic rocks, as well as their relatively thin veneer of sediments, into a subduction zone can liberate considerable amounts of fluid via devolatilization reactions that occur during prograde metamorphism of the subducted materials (e.g. You *et al.*, 1996; Bebout *et al.*, 1999; Becker *et al.*, 1999, 2000; Gao & Klemd, 2001; Rüpke *et al.*, 2004).

According to Peacock (1993a), the transition from blueschist to eclogite is considered as the main reaction that produces large amounts of H₂O by the continuous breakdown of hydrous minerals such as lawsonite, chlorite, clinozoisite–epidote and Na-amphibole to an anhydrous garnet + omphacite assemblage. Other models, however, imply that a large portion of the H₂O is liberated at relatively shallow depths in the subduction zone (Philippot, 1993), or that many different reactions modify the water content of hydrous phases during the transition from blueschists to anhydrous eclogites, which may occur simultaneously in different portions of the subducting slab (Schmidt & Poli, 1998). Owing to the low density of H₂O

compared with the surrounding rocks, the H₂O released will tend to migrate upwards into the mantle wedge or along the surface of the subducted slab (Peacock, 1990). Zack & John (2007) have emphasized the importance of fluid channelization, as the permeability of the subducting slab is considered to be too low.

Large-scale fluid flow has been documented in metasedimentary, metabasic and meta-ultrabasic rocks from three tectono-metamorphic units of lawsonite–albite-to amphibolite-facies grade in the Catalina Schist (California) by Bebout *et al.* (1999). On the basis of their whole-rock trace element compositions [B/(Be, Li, La, Zr), Cs/Th, Rb/Cs, As/Ce] they demonstrated that the most extensive devolatilization occurs in the forearc in metasedimentary rocks that have experienced a prograde *P–T* path up to epidote-blueschist-facies conditions. Based on geochemical depth profiles, Ryan *et al.* (1996) showed that trace element abundances in the Catalina Schist change with slab depth. Decreases in B and Cs contents correlate with decreases in H₂O, suggesting that an H₂O-rich fluid was the medium in which these species were removed (Bebout *et al.*, 1999).

Mobilization of trace elements in the subduction zone during devolatilization is considered to be an important process for the enrichment of large ion lithophile elements (LILE) and light rare earth elements (LREE) relative to heavy rare earth elements (HREE) and high field strength elements (HFSE) in arc magmas (e.g. Tribuzio *et al.*, 1996; Becker *et al.*, 2000; Scambelluri & Philippot, 2001; Zack *et al.*, 2002; Spandler *et al.*, 2003, 2004; Miller *et al.*, 2007).

John *et al.* (2004) have shown that trace elements can be mobilized in eclogites that have interacted with high amounts of fluids. For example, John *et al.* (2007) reported from Tianshan in China that infiltration of an external fluid in a vein under eclogite-facies conditions triggered eclogitization of the blueschist host by interaction with the passing fluid. During this fluid–rock interaction, the infiltrating fluid was able to mobilize 40–80% of the LILE, REE and HFSE from the host-rock. Thus, channelized fluid flow could transport significant amounts of LILE into the overlying mantle wedge.

On the basis of trace element studies of whole-rocks and metamorphic minerals Tribuzio *et al.* (1996), Zack *et al.* (2001, 2002), Spandler *et al.* (2003), and Miller *et al.* (2007) observed a decoupling between trace element migration and fluid loss during devolatilization. This implies that trace element abundances are controlled by the presence and stabilities of certain minerals and that the mobilization of trace elements is low during the slab dehydration process. Significant amounts of LILE and LREE may be transported in the subduction zone to a depth of 70–150 km, because of the large stability range of phengite and biotite (Hermann & Green, 2001; Spandler *et al.*, 2004). At these depths, the LREE and

LILE can be released because of the breakdown of epidote and phengite (Becker *et al.*, 2000).

This study examines the distribution of incompatible trace elements and REE in the metamorphic mineral assemblages of eclogite-, blueschist- and greenschist-facies rocks occurring in the Ile de Groix (Brittany, France) to better understand the geochemical fingerprint that fluid mobilization imparts on the rock during dehydration and rehydration processes. Epidote-group minerals, lawsonite, garnet, phengite, titanite, rutile and apatite constitute the main minerals of interest for the trace element budget and recycling (Hermann, 2002; Zack *et al.*, 2002; Spandler *et al.*, 2003; Miller *et al.*, 2007; Usui *et al.*, 2007). This study places particular emphasis on the importance of trace element exchange between minerals during the various stages of the metamorphic cycle in relation to the mineral stabilities and reactions along the P - T path.

GEOLOGY

The Ile de Groix forms the outcropping part of a submergued Hercynian HP-LT metamorphic belt located off the southern coast of Brittany (Audren & Lefort, 1977). The HP rocks are interpreted as the remnants of a Palaeozoic accretionary prism (Ballèvre *et al.*, 1998) and consist of around 80% pelitic and 20% basic lithologies, intercalated at all scales (Fig. 1). The dimensions of the basic bodies, which sometimes exhibit isoclinal folds or boudinage, vary from lens of a few centimetres to metre scale to layers of several tens of metres (Audren *et al.*, 1993; Bosse *et al.*, 2002; Ballèvre *et al.*, 2003).

Petrological studies on the metapelites (Djro *et al.*, 1989; Bosse *et al.*, 2002), as well as on the basic rocks (Triboulet, 1974; Carpenter, 1976; Audren & Triboulet, 1984, 1993; Barrientos, 1992; Barrientos & Selverstone, 1993; Schulz *et al.*, 2001; Ballèvre *et al.*, 2003), indicate two metamorphic events: a blueschist-eclogite-facies metamorphism (M_1) related to subduction, and a greenschist-facies overprint during exhumation (M_2), which is dominant in the western part of the island.

Two main domains of deformation with different structures have been characterized (Cogné *et al.*, 1966; Boudier & Nicolas, 1976; Carpenter, 1976; Quinquis, 1980; Quinquis & Choukroune, 1981): flat-lying or gently dipping foliations and a NNW-SSE-trending stretching lineation are present in the eastern part of the island, whereas the western part is formed by a major antiformal fold, with an axis oriented NW-SE. The first deformation event (D_1) is characterized by progressive deformation responsible for a blueschist-facies foliation S_1 , defined by the growth of glaucophane, epidote and phengite in basic rocks, and chloritoid in metapelites. Deformation started during the prograde path and a HP-LT event (M_1) and continued during the beginning of the retrogression (M_2). A second phase of deformation (D_2) took place during retrograde

greenschist-facies metamorphism, deforming S_1 and resulting in the formation of a large-scale N130-140-trending antiform and a crenulation cleavage S_2 . Blueschist-facies parageneses, in basic rocks as well as in the micaschists, are overprinted essentially by an assemblage of chlorite, albite and magnetite (Bosse *et al.*, 2005).

For the metapelites, the P - T peak conditions in the blueschist facies have been determined to be 1.6-1.8 GPa, 450-500°C in the eastern part of the island, and 1.4-1.6 GPa, 400-450°C in the western part using the NFMASH system (Bosse *et al.*, 2002). In the basic rocks of the eastern part of the island, Ballèvre *et al.* (2003) have estimated peak conditions for the blueschist-facies rocks of 1.8-2.0 GPa, at 450°C using THERMOCALC, based on the presence of lawsonite pseudomorphs.

The high-pressure event (blueschist facies) has been dated at 358-365 Ma with the $^{40}\text{Ar}/^{39}\text{Ar}$ (phengite) and Rb-Sr (whole-rock, phengite and epidote) methods, whereas a younger age of 345-353 Ma was determined for the greenschist metamorphic event using the same methods (Bosse *et al.*, 2005). This implies that the exhumation rate was fast, as has often been observed in other orogens, such as the Western Alps (e.g. Agard *et al.*, 2008), Caucasus (Perchuk & Philippot, 1997) or Tianshan (Gao & Klemd, 2003).

Based on the mineral assemblages and metamorphic facies, the metabasites of the Ile de Groix have been traditionally subdivided into (1) eclogites or omphacite-bearing blueschists, (2) blueschists, sometimes partially amphibolitized, and (3) greenschists (Audren *et al.*, 1993). The blueschist-facies metabasites represent peak metamorphic assemblages and show no evidence of eclogitization. A few samples correspond to blueschist-facies overprinted eclogites, as revealed by the presence of omphacite pseudomorphs formed by symplectites of barroisite and albite (eclogite GR 21). All the greenschist-facies rocks have experienced a retrogression from HP rocks, but there is no evidence as to whether these samples were originally blueschists or partially eclogitized blueschists. The difference in mineral parageneses between the eclogites and blueschists is explained by small variations in the composition of the protoliths and by small differences in temperature (50-75°C) for the peak metamorphic conditions in the subducting slab (Peacock, 1993a). Amongst the blueschist- and greenschist-facies metabasites, both massive and banded lithologies can be distinguished (El Korh, 2006; El Korh *et al.*, 2007, 2009; Schmidt *et al.*, 2008).

SAMPLING

Fifteen samples were studied, typical of each metamorphic facies and textural type; these include nine massive basic rocks (eclogites GR 21, 24a and 29; blueschists GR 02, 11b, 12b and 25a; greenschists GR 23, 25b and 27a), four banded basic rocks (blueschist-facies GR 12a, 28 and 31;

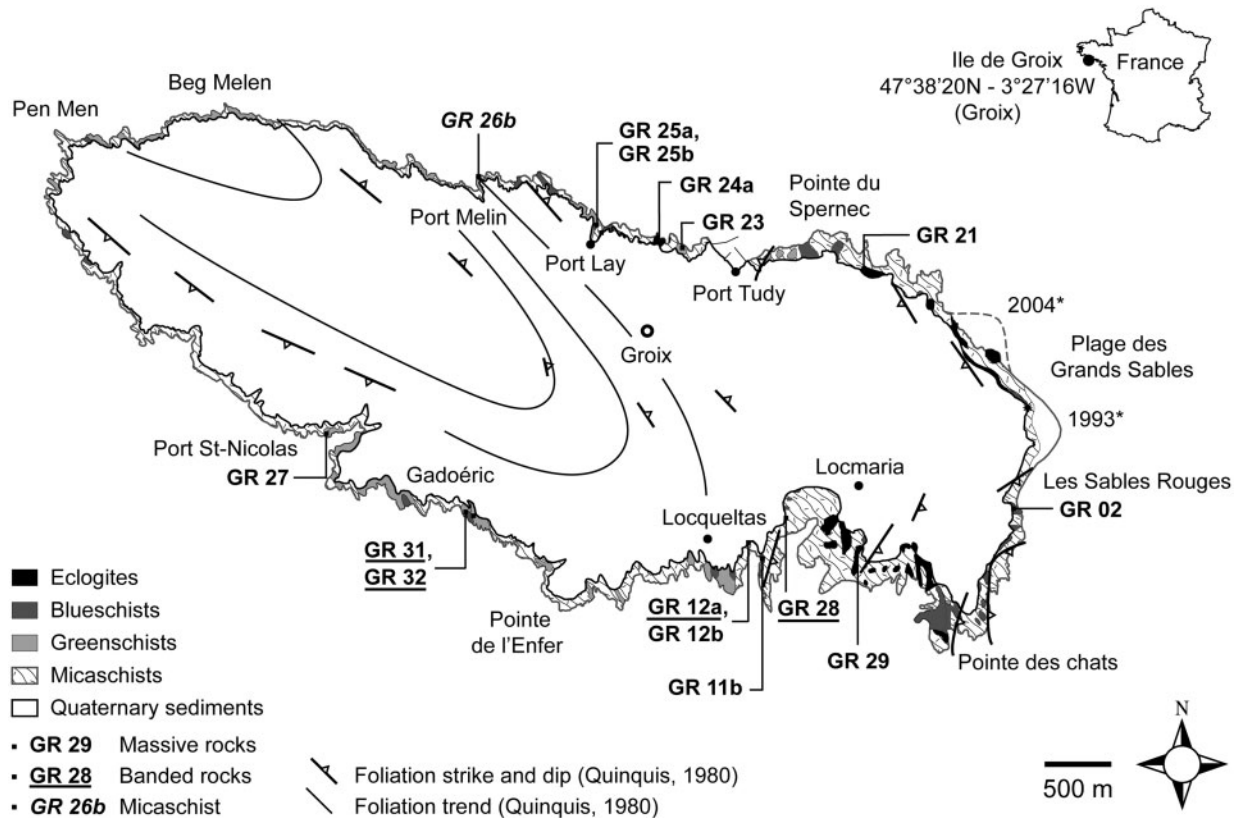


Fig. 1. Geological map of the Ile de Groix, based on Audren *et al.* (1993), Bosse *et al.* (2005) and El Korh (2006). The beach 'Plage des Grands Sables' moves periodically because of the currents. 1993* corresponds to its position on the geological map by Audren *et al.* (1993), and 2004* refers to its position based on our field observations.

greenschist-facies GR 32) and one metapelite (GR 26b) collected from all around the island, mainly along the well-exposed shore-line (Fig. 1 and Table 1 for mineralogical characteristics). Most of the outcrops are composed of an alternation of different lithologies. Two to ten cubic decimetres of homogeneous samples were recovered, depending on the accessibility and the homogeneity of the outcrops. Several samples were collected from adjacent outcrops (Fig. 1; Table 1). Four massive rocks were sampled from the northern part of the island: massive blueschist GR 25a in direct contact with massive greenschist GR 25b, eclogite GR 24a and massive greenschist GR 23. In the southern part of the island, two closely related rocks of different facies (banded blueschist GR 31 and greenschist GR 32, in the west) or textural type (banded blueschist GR 12a and massive blueschist GR 12b, in the east) were collected.

ANALYTICAL TECHNIQUES

Whole-rock compositions

Whole-rock major element compositions of the metamorphic rocks were determined by X-ray fluorescence

spectrometry (XRF) using a Philips PW2400 instrument at the Centre of Mineral Analysis at the University of Lausanne. Loss on ignition (LOI) values were quantified based on the mass difference of a 2.5–3 g powdered rock aliquot before and after heating to 1050°C. Trace elements abundances were analysed on fused lithium tetraborate glass discs by laser ablation inductively coupled plasma mass-spectrometry (LA-ICPMS) at the Institute of Mineralogy and Geochemistry, University of Lausanne. The LA-ICPMS instrument is equipped with a GeoLas 200M 193 nm ArF excimer laser ablation system (Lambda Physik, Germany) interfaced to an ELAN 6100 DRC quadrupole ICPMS (Perkin Elmer, Canada). Operating conditions of the laser included a 140 mJ output energy (equivalent to *c.* 10 J/cm² on-sample fluence), 10 Hz repetition rate and 120 µm pit size. Helium was used as the cell gas. The acquisition times for the background and the ablation interval were *c.* 70 and 30–35 s, respectively. Dwell times per isotope ranged from 10 to 20 ms, and peak-hopping mode was employed. The ThO⁺/Th⁺ and Ba²⁺/Ba⁺ ratios were optimized to *c.* 0.6 and 2.0–2.7%, respectively. The NIST 612 reference material, representing a synthetic glass doped with trace elements, was used for external standardization. The average element abundances

Table 1: Provenance, mineralogical and textural characteristics and inferred protoliths of the studied HP–LT metamorphic rocks

Sample	Locality*	Coord. x/y UTM (m)	Facies	Texture	Protolith	Mineralogy†
GR 21	Poskedoul	467512/5276718	Eclogite	Massive	MORB	Grt-gln-omph-barr-ep-phe-chl-qtz-Fe ox (hm)
GR 24a	Plage du Rolaz	465785/5276945	Eclogite	Massive	MORB	Grt-gln-barr-ep-omph-phe-chl-qtz-Fe ox (hm, mt)
GR 29	Porh Giguéou	467382/5274810	Eclogite	Massive	MORB	Grt-gln-omph-barr-ep-phe-chl-qtz-ap-rt-ttn-± ◇ lws
GR 02	Les Sables Rouges	468550/5275006	Blueschist	Massive	MORB	Grt-gln-barr-ep-phe-qtz-ttn-rt-ap-◇ lws
GR 11b	Les Saisies	466697/5274607	Blueschist	Massive	AB/MORB?	Grt-gln-barr-ep-phe-chl-ab-ttn-Fe ox (mt)-◇ lws
GR 12b	Porh Roëd	466646/5274714	Blueschist	Massive	AB/MORB?	Gln-act-ep-phe-chl-ab-ttn-ap-qtz-Fe ox (hm)-◇ lws
GR 25a	Port Lay	465455/5277071	Blueschist	Massive	MORB	Grt-gln-ep-phe-act-qtz-chl-ttn-Fe ox (mt)-◇ lws
GR 23	Côte d'Héno	466150/5276845	Greenschist	Massive	MORB	Grt-ep-chl-ab-barr-phe-act-gln-ttn-rt-Fe ox (mt)-◇ lws
GR 25b	Port Lay	465455/5277071	Greenschist	Massive	MORB	Grt-ep-chl-gln-barr-act-ab-qtz-ap-ttn-rt-Fe ox (mt)-◇ lws
GR 27a	Port St-Nicolas	463542/5275570	Greenschist	Massive	AB/MORB?	Grt-ep-chl-act-ab-phe-barr-ttn-rt-◇ lws
GR 12a	Porh Roëd	466646/5274714	Blueschist	Banded	VS	Grt-phe-gln-ep-ttn-rt-ap-qtz-Fe ox (hm)
GR 28	Kermarec	466793/5274848	Blueschist	Banded	VS	Grt-gln-cross-barr-ep-phe-chl-ab-qtz-ttn-rt-mt-Fe-Ti ox
GR 31	Gadoëric	464448/5275025	Blueschist	Banded	VS	Ep-cross-gln-barr-chl-phe-ttn-plag-ap-qtz-Fe ox (mt)
GR 32	Gadoëric	464460/5274995	Greenschist	Banded	VS	Ep-phe-chl-ab-cross-barr-ttn-ap-tur-Fe ox (mt)
GR 26b	Port Melin	464578/5277376	Greenschist	Schistose	Pelitic	Grt-phe-ep-qtz-chl-bt-ab-ttn-ap-Fe ox (mt, hm)-tur

MORB, mid-ocean ridge basalt; AB, alkaline basalt; VS, volcano-sedimentary rock. ◇ lws, pseudomorphs after lawsonite.

*See Fig. 1.

†The mineral abbreviations are from Kretz (1983).

in the glass were taken from Pearce *et al.* (1997). Intensity vs time data were reduced using LAMTRACE, a Lotus 1–2–3 spreadsheet written by Simon Jackson (Macquarie University, Australia). ⁴²Ca served as an internal standard.

Compositions of minerals

Major element compositions of minerals were analysed by wavelength-dispersive analysis using five-spectrometer CAMECA SX50 and JEOL JXA-8200 electron microprobes at the Institute of Mineralogy and Geochemistry, University of Lausanne. Control measurements performed on both instruments proved to be consistent. The accelerating voltage and the beam current were set at 15 kV and 15 nA, respectively. The counting times were 10 s for alkalis, F and Cl and 20 s for other elements. The beam size ranged from 1 to 10 µm. Raw data were reduced using the PAP routine. All iron was calculated as Fe²⁺ in garnet, phengite, chlorite and apatite and as Fe³⁺ in epidote, titanite and rutile. In amphibole and omphacite, Fe²⁺, Fe³⁺ and water contents were calculated assuming ideal stoichiometry.

Most trace element analyses were performed during the period 2006–2008 using the same quadrupole LA-ICPMS instrument as for the whole-rock glass discs. Ablation pit sizes ranged from 30 to 100 µm, depending on the grain size of the minerals and their trace element abundances.

The output energy varied from 120 to 170 mJ (equivalent to *c.* 10 to 34 J/cm² on-sample fluence, respectively). The elevated output energy values were applied, particularly in late 2006, to partially compensate for the gradual decrease of on-sample laser fluence caused by the degradation of the optical parts of the ablation system with time between its refurbishments. The acquisition times for the background and the ablation interval were *c.* 70 and 15–25 s, respectively. External standards were the NIST 612 and 610 synthetic glasses. Most analyses were standardized against the NIST 612 glass. The NIST 610 glass was used mainly for the analysis of titanite, rutile and iron oxides. Other parameters of the instrument set-up were similar to those discussed above for the glass discs. Internal standards were ⁴²Ca (epidote, apatite, omphacite), ²⁷Al (garnet, phengite, glaucophane, barroisite, actinolite, chlorite, albite), ⁴⁹Ti (titanite, rutile) and ⁵⁷Fe (iron oxides).

Trace element contents in garnet, omphacite, phengite and amphibole were additionally analysed using an Element XR sector field ICPMS system (ThermoFisher Scientific, Germany and USA) interfaced to an UP193-FX ArF 193 nm excimer ablation (New Wave Research, USA) recently installed at the Institute of Mineralogy and Geochemistry, University of Lausanne. Operating conditions of the laser included an output energy of 8 mJ (equivalent to 5 J/cm² on-sample fluence), 20 Hz repetition

rate and 75–150 μm pit sizes. Helium was used as a cell gas. The acquisition times for the background and the ablation interval were *c.* 70 and 60 s, respectively. Almost all isotope masses were scanned using four acquisition points per peak, the mass window having been set at 20% of the peak width. Dwell times per point were 5 ms for ^{42}Ca and ^{27}Al and 10 ms for trace elements. The ThO^+/Th^+ and $\text{Ba}^{2+}/\text{Ba}^+$ ratios were optimized to *c.* 0.1–0.2% and 1.0–1.4%, respectively. The NIST 612 synthetic glass was used for external standardization. ^{27}Al served as an internal standard.

Intensity vs time data from both ICP instruments were reduced in LAMTRACE. They were checked for the presence of intensity ‘spikes’ and corrected when necessary. The average element values in the NIST 610 and 612 glasses were taken from Pearce *et al.* (1997).

Minerals showing chemical zoning (e.g. epidote and garnet) were studied in detail by using electron microprobe profiles and a large amount of LA-ICPMS data, whereas only a few analyses were necessary to characterize the homogeneous minerals (e.g. omphacite, titanite, amphiboles, chlorite and plagioclase). Inclusions in minerals were avoided during analysis as much as possible.

PETROGRAPHY

Eclogites (or omphacite-bearing blueschists)

The metamorphic assemblage of the eclogites (GR 21, GR 24a and GR 29) includes garnet, omphacite, glaucophane, epidote, phengite, apatite, quartz and rutile (Table 1). These are medium-grained massive rocks, which do not seem to have experienced total eclogitization during the HP event. Euhedral poikiloblasts of garnet contain frequent inclusions of titanite, epidote, quartz, apatite, zircon, glaucophane and omphacite (Fig. 2a and b). Anhedral omphacite forms lenses surrounded by the schistose matrix. In thin section, the schistosity is well defined by glaucophane and epidote. Three generations of epidote can be distinguished based on textural and optical characteristics. Epidote I forms small crystal aggregates. Epidote II constitutes the rims of these aggregates or cores of larger crystals in the matrix. Epidote III forms rims around epidote II or small crystals in the matrix. Pseudomorphs after lawsonite are sometimes present (GR 29). The phengite content in the eclogites is low (<3–4%). Retrogression textures include barroisite overgrowths on rims of glaucophane, barroisite and albite symplectite overgrowths on omphacite, and partial replacement of garnet by chlorite and rutile by titanite (Fig. 3a and b). Iron oxides also crystallized during the retrogression. Eclogite GR 29 appears less retrogressed than eclogite GR 24a, in which most of the rutile has been replaced by

titanite. Eclogite GR 21 shows strong indication of greenschist-facies rehydration.

Massive blueschists

Blueschists are massive rocks of fine to medium grain size (GR 02, GR 11b, GR 12b) sometimes displaying alternating layers dominated by glaucophane or epidote (GR 25a). In thin section they show a well-developed foliation. The metamorphic assemblage consists of garnet, glaucophane, epidote, phengite, apatite, rutile, titanite and quartz (Fig. 2c–f; Table 1). Pseudomorphs of lawsonite include epidote, white mica (phengite, paragonite), actinolite, albite and/or chlorite (Fig. 2g and h). Garnet occurs as euhedral crystals (GR 02, GR 11b, GR 25a). It is rich in inclusions such as epidote, rutile and quartz in GR 02, titanite and epidote in GR 11b, and titanite, epidote and apatite in GR 25a (Fig. 2c and d). Retrogression is evident from overgrowths of barroisite (GR 02, GR 11b, GR 25a) and actinolite (GR 12b) on glaucophane, limited replacement of garnet by chlorite (GR 11b, GR 25a), partial replacement of rutile by titanite (GR 02 and GR 25a; Fig. 3c), and formation of albite (GR 11b).

Up to three generations of epidote—often optically recognizable—can be distinguished in the blueschists. In blueschist GR 02, two epidote generations (Fig. 2e and f) are distinguished: epidote I formed in the core and epidote II along the rims. In massive blueschist GR 11b three generations of epidote occur. Epidote I forms cores of small crystals in the matrix. Epidote II constitutes small grains in lawsonite pseudomorphs and rims of small crystals in the matrix. Epidote III forms small isolated crystals in the matrix and can be distinguished from epidote II based on its trace element composition (see the section on ‘Mineral chemistry’). In blueschist GR 12b, epidote I crystallized in the matrix in equilibrium with glaucophane. Epidote II and III are optically zoned and are related to pseudomorphs after lawsonite. In blueschist GR 25a, epidote I forms the core part of a large prograde relict Fe-rich epidote crystal, epidote II represents the core part of smaller crystals in the matrix and epidote III is the last generation occurring at the rim. Two generations of titanite are observed in GR 25a: titanite I occurs in the matrix and titanite II is commonly associated with the lawsonite pseudomorphs. Prograde apatite surrounded by the schistosity is observed only in GR 02.

Massive greenschists

The massive greenschists GR 23, GR 25b and GR 27a (Table 1) are fine to medium grained and are considered to be highly retrogressed blueschists. They display an assemblage of garnet, epidote, chlorite, actinolite, barroisite, albite, magnetite (partially resorbed by hematite), titanite and rutile as well as rare relicts of glaucophane

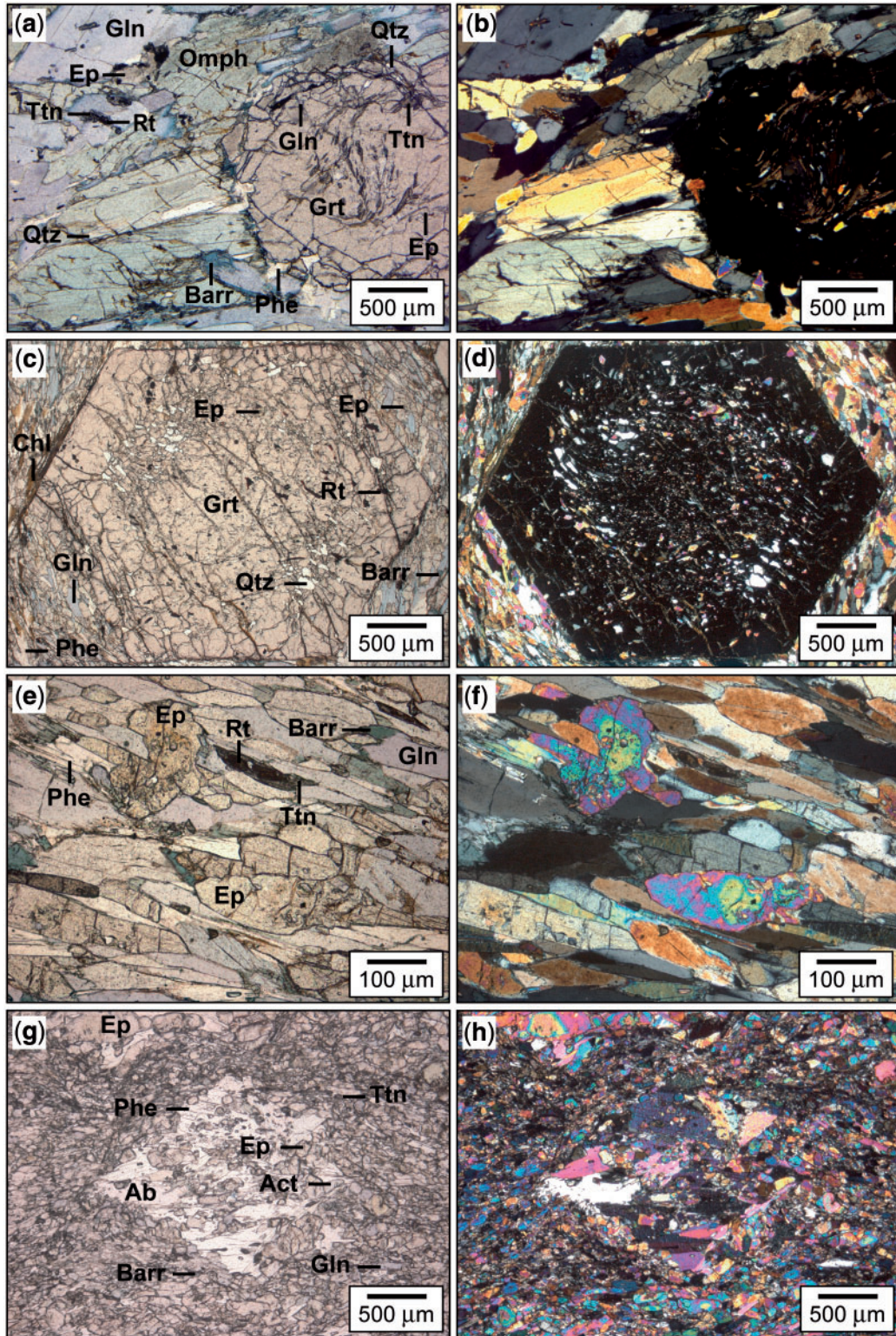


Fig. 2. Photomicrographs representing different aspects of prograde minerals. (a, b) Typical garnet–omphacite–glaucophane assemblage of eclogite GR 29. The euhedral poikiloblast of garnet contains inclusions of titanite, epidote, quartz and glaucophane. Barroisite overgrowths are present on the rims of glaucophane. (c, d) Euhedral poikiloblast of garnet with inclusions of rutile, epidote and quartz in massive blueschist GR 02. (e, f) Zoned epidote, rutile rimmed by titanite and glaucophane rimmed by barroisite in massive blueschist GR 02. (g, h) Lawsonite pseudomorphs composed of phengite, epidote, actinolite and albite in massive blueschist GR 12b. Left-hand panels in plane-polarized light; right-hand panels in cross-polarized light.

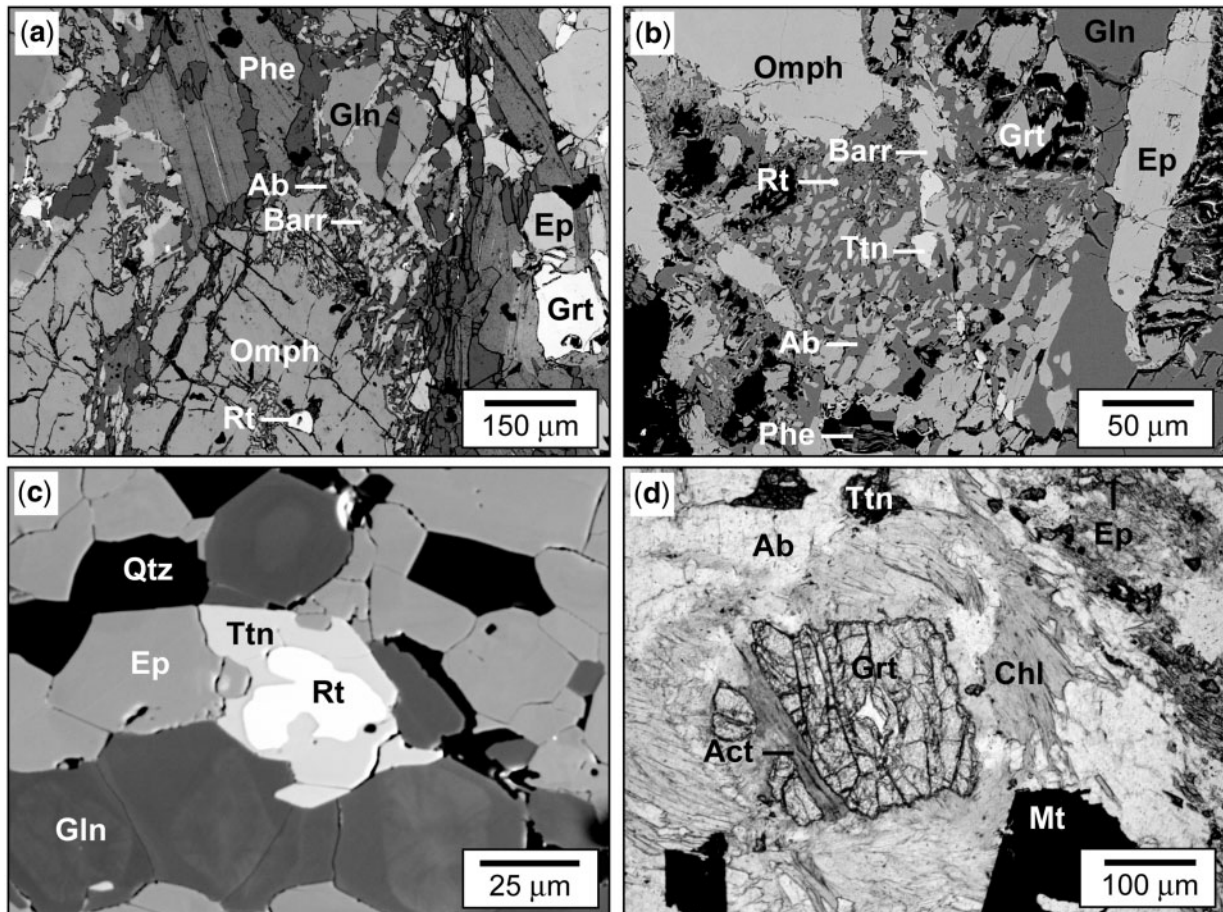


Fig. 3. Typical retrograde overprints. (a, b) Backscattered SEM images of albite and barroisite symplectite overgrowths on omphacite in massive eclogites GR 29 and GR 21. (c) Backscattered SEM image of titanite overgrowth on rutile in the rock matrix of massive blueschist GR 02. (d) Typical retrograde assemblage of massive greenschist GR 23 composed of albite, chlorite, actinolite and magnetite replacing garnet (see the section 'Petrography').

rimmed by a retrograde assemblage of barroisite (GR 23) or barroisite and actinolite (GR 25b, GR 27a). Garnet is largely replaced by chlorite, actinolite and epidote in GR 23 (Fig. 3d) and by chlorite in GR 25b and GR 27a. It contains small inclusions of titanite and epidote (GR 27a).

Epidote shows different generations of growth. In massive greenschist GR 23, epidote I corresponds to layered domains of epidote, epidote II constitutes the core parts of large epidote crystals in association with garnet, epidote III forms the largest crystals in the rock and seems to be retrograde, and epidote IV rims epidote II and III. Epidote in the massive greenschist GR 25b forms two generations in the matrix: epidote I in the cores and epidote II at the rims. In massive greenschist GR 27a, two generations of epidote are observed, but no evidence of prograde epidote was recognized. The two generations of epidote can be related to epidote II and III defined in the two

other massive greenschists. Post-lawsonite epidote II occurs at the rims of lawsonite pseudomorphs and contains numerous inclusions. Retrograde epidote III occurs as isolated grains in the matrix. Two generations of titanite are present in GR 25b and GR 27a.

Banded blueschists and greenschists

The fine- to medium-grained banded blueschists GR 12a, GR 28 and GR 31 and greenschist GR 32 are macroscopically characterized by alternation of layers of varying size and dominated either by elongated grains of glaucophane–crossite and/or chlorite, either by epidote and phengite (Table 1). In thin section, these rocks are generally well foliated. Subidiomorphic garnet (GR 12a and GR 28), titanite, rutile, apatite, quartz and oxides are also present, as well as accessory tourmaline (Table 1). Garnet possesses small inclusions of epidote, titanite, quartz and

apatite, which are smaller and less frequent than in garnet from the massive rocks. Glaucophane and epidote are optically zoned. Glaucophane crystals are usually large and well shaped, whereas the size of the epidote crystals varies significantly. Epidote displays two generations. In GR 12a, epidote I forms fine-grained epidote layers, which are sometimes folded and often highly fractured. Epidote II forms larger crystals. In GR 28, epidote I forms small crystals and cores of larger crystals, whereas epidote II corresponds to rims of large crystals. In GR 31, epidote I forms small crystals and is sometimes rimmed by epidote II, especially in greenschist GR 32.

Retrogression is present to various degrees, such as the replacement of rutile by titanite (GR 12a and GR 28), the crystallization of albite including previously formed minerals oriented according to the schistosity, chlorite and iron oxides (magnetite) in the matrix and overgrowths of barrosite after glaucophane and crossite (GR 28, GR 31 and GR 32). The banded greenschist GR 32 represents a retrogressed equivalent of a blueschist similar to GR 31 (Table 1), which is expressed by the almost complete replacement of crossite by chlorite and barrosite.

Metapelite

Well-foliated greenschist-facies metapelite GR 26b consists of phengite, garnet, quartz, chlorite, albite, epidote, titanite, apatite, biotite and iron oxides. Accessory tourmaline is present (Table 1). Garnet porphyroblasts are partially replaced by chlorite and contain many small inclusions of titanite and epidote. Epidote forms three generations: epidote I corresponds to the cores of large elongated crystals, epidote II forms rims on epidote I grains and small crystals, and epidote III appears as small isolated crystals. Phengite displays two generations: phengite I forming the schistosity and postkinematic phengite II. Epidote, titanite and apatite are important hosts for trace elements despite their low modal abundance.

WHOLE-ROCK CHEMISTRY

Major elements

Major and trace element compositions of the 15 studied samples are given in Table 2. SiO₂ contents range from 46.6 to 51.0 wt % and are similar in both massive and banded rocks. Al₂O₃ content varies from 13.7 to 17.7 wt % in the massive rocks and from 14.7 to 18.5 wt % in the banded rocks. The main chemical differences between the massive and banded basic rocks are in their MgO and K₂O contents (Fig. 4): MgO contents are generally higher in the massive rocks (5.0–6.6 wt %, except GR 02: 4.1 wt %) than in the banded rocks (2.3–3.3 wt %, except GR 31: 6.1 wt %), and K₂O contents are low in the massive

rocks (0.1–0.9 wt %) and high in the banded rocks (1.0–3.8 wt %). Na₂O values range from 2.7 to 4.5 wt % in the massive rocks and from 1.1 to 3.5 wt % in the banded rocks. Micaschist GR 26b displays high SiO₂, Al₂O₃ and K₂O (50.1, 21.3 and 5.1 wt %, respectively) and low MgO (2.3 wt %) and Na₂O (0.7 wt %) contents. The LOI values range from 0.9 to 3.2 wt % (3.4 wt % in micaschist GR 26b). Higher values correlate with increasing degrees of retrogression.

Trace elements

Primitive mantle (PM)-normalized multi-element diagrams (Fig. 5) are used to compare the studied samples with normal (N)-MORB, enriched (E)-MORB, ocean island basalts (OIB) and upper crust (Sun & McDonough, 1989) and with the composition of Global Oceanic Subducting Sediment (GLOSS; Plank & Langmuir, 1998). The patterns show that all the rocks studied are enriched in incompatible trace elements, especially LILE, compared with N-MORB (Fig. 5). The trace element patterns of the massive rocks are generally similar to those of E-MORB, with significant variations in LILE content between samples (Fig. 5a). Some samples (GR 02, GR 12b, GR 27a and GR 29) display a positive Pb anomaly (Fig. 5a). Most of the massive rocks display a negative Nb anomaly. Ba negative anomalies are also observed in eclogite GR 29 as well as in the greenschist-facies rocks. The banded rocks are compositionally heterogeneous and plot between the E-MORB and the upper crust reference patterns (Fig. 5b). The banded greenschist GR 32 displays a pattern similar to those of the massive rocks and E-MORB, whereas the banded blueschists GR 31 and particularly GR 12a and GR 28 are more enriched in LILE and LREE, approaching the GLOSS and upper crust patterns (Fig. 5b; Table 2). Pb is often strongly enriched in the banded rocks. The primitive mantle-normalized trace element pattern of micaschist GR 26b (Fig. 5c) shows fractionation of LILE and LREE over HFSE and HREE and is similar to the upper crust pattern and to GLOSS containing 76% of terrigenous material (Plank & Langmuir, 1998).

The primitive mantle-normalized REE patterns (Fig. 6) show little fractionation of REE in the majority of the massive rocks [(Ce/Yb)_{PM} ~ 1.2–1.5; Fig. 6a] as is the case for MORB [(Ce/Yb)_{PM} in N-MORB ~ 0.7 and in E-MORB < 1.8], except for samples GR 11b [(Ce/Yb)_{PM} ~ 2.4], GR 12b [(Ce/Yb)_{PM} ~ 6.4], and GR 27b [(Ce/Yb)_{PM} ~ 4.4]. On the other hand, the LREE are enriched in most banded rocks [e.g. GR 12a, GR 28 and GR 31: (Ce/Yb)_{PM} ~ 3.3–4.1; Fig. 6b] and in micaschist GR 26b [(Ce/Yb)_{PM} ~ 3.9; Fig. 6c]. Nevertheless, the LREE enrichment in these rocks is less marked than in GLOSS [(Ce/Yb)_{PM} ~ 5.8].

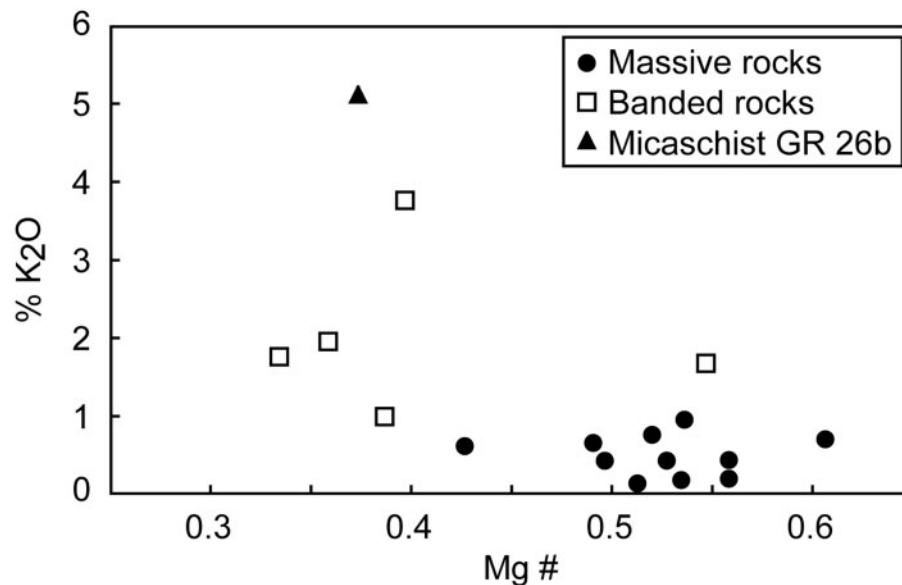


Fig. 4. Mg-number vs K₂O diagram for massive rocks and banded rocks of all metamorphic facies and micaschist GR 26b.

MINERAL CHEMISTRY

Major elements

Amongst the studied samples, garnet shows strong variations in major element content whereas other minerals only display minor variations (Table 3). In all samples, the garnet composition is dominated by the almandine component (60–70%). Garnet is often zoned, particularly in the banded rocks, displaying rimward enrichment in the almandine component and depletion in the spessartine component; this is typical of garnet formed during prograde metamorphism (Fig. 7; Table 3). This typical zonation pattern is absent in the garnet in blueschist GR 02, the cores being slightly richer in almandine and spessartine. Epidote compositions belong to the clinzoisite–epidote solid solution series. In eclogites, epidote major element compositions show only small variations in each sample (Table 3) and from one rock to another ($X_{Fe^{3+}} \sim 19$ –25%). In massive blueschists, massive greenschists and banded rocks, epidote generally displays an Fe–Al zonation defined by a rimward increase in the clinzoisite component ($X_{Fe^{3+}} \sim 32$ –19%); Fe-rich epidote I and II ($X_{Fe^{3+}} \sim 30$ –32%) are rimmed by Fe-poorer epidote III ($X_{Fe^{3+}} \sim 19$ –24%) and IV ($X_{Fe^{3+}} \sim 23$ –24%; greenschist GR 23). In greenschist GR 27a, epidote I and II are enriched in Al ($X_{Fe^{3+}} \sim 10$ –17%). The three epidote generations in micaschist GR 26b are compositionally similar for the major elements ($X_{Fe^{3+}} \sim 19$ –25%). Omphacite contains 43–53% of augite, 10–11% of aegirine and 36–46% of jadeite components (Table 3). Phengite composition is relatively homogeneous in individual samples, but varies from one sample to another ($X_{Al^{VI}} 73$ –84%; Mg-number

41–76%). Blue amphiboles generally correspond to glaucophane (Mg-number ~ 79 –92%; $X_{Fe^{3+}} \sim 31$ –41%), or display a rimward zonation from crossite (Mg-number ~ 70 –76%; $X_{Fe^{3+}} \sim 37$ –43%) to glaucophane in banded rocks (Table 3).

Trace elements

Trace elements were analysed in all minerals of the studied rocks (Figs 8–12; Tables 4–8). All minerals generally contain high contents of compatible trace elements (Sc, V, Cr, Co, Ni, Zn, Ga). The main hosts of incompatible trace elements are garnet (Y, HREE), epidote (REE, Th, U, Pb, Sr), phengite (Cs, Rb, Ba, B, Li), titanite (Ti, Nb, Ta, REE; HREE > LREE), rutile (Ti, Nb, Ta) and apatite (REE, Sr). Chondrite-normalized trace element patterns of the minerals and scatterplots for phengite are shown in Figs 8–12. Epidote plays a central role in the trace element exchange because of its large stability field during metamorphism. Trace element contents in omphacite, glaucophane, barroisite, actinolite, albite, chlorite and iron oxides are generally low, often below or close to the detection limits, excepted for Li, B and Be (Table 8). Retrograde albite contains high contents of Sr and easily measurable amounts of Cs, Rb, Ba and Pb. Although these minerals constitute an important part of the assemblage of the basic rocks from the various metamorphic facies, they do not play an important role in the bulk-rock budget for incompatible trace elements. The detailed description of major and trace element compositions of the main trace element hosting minerals and a larger set of analyses are available as Electronic Appendices at

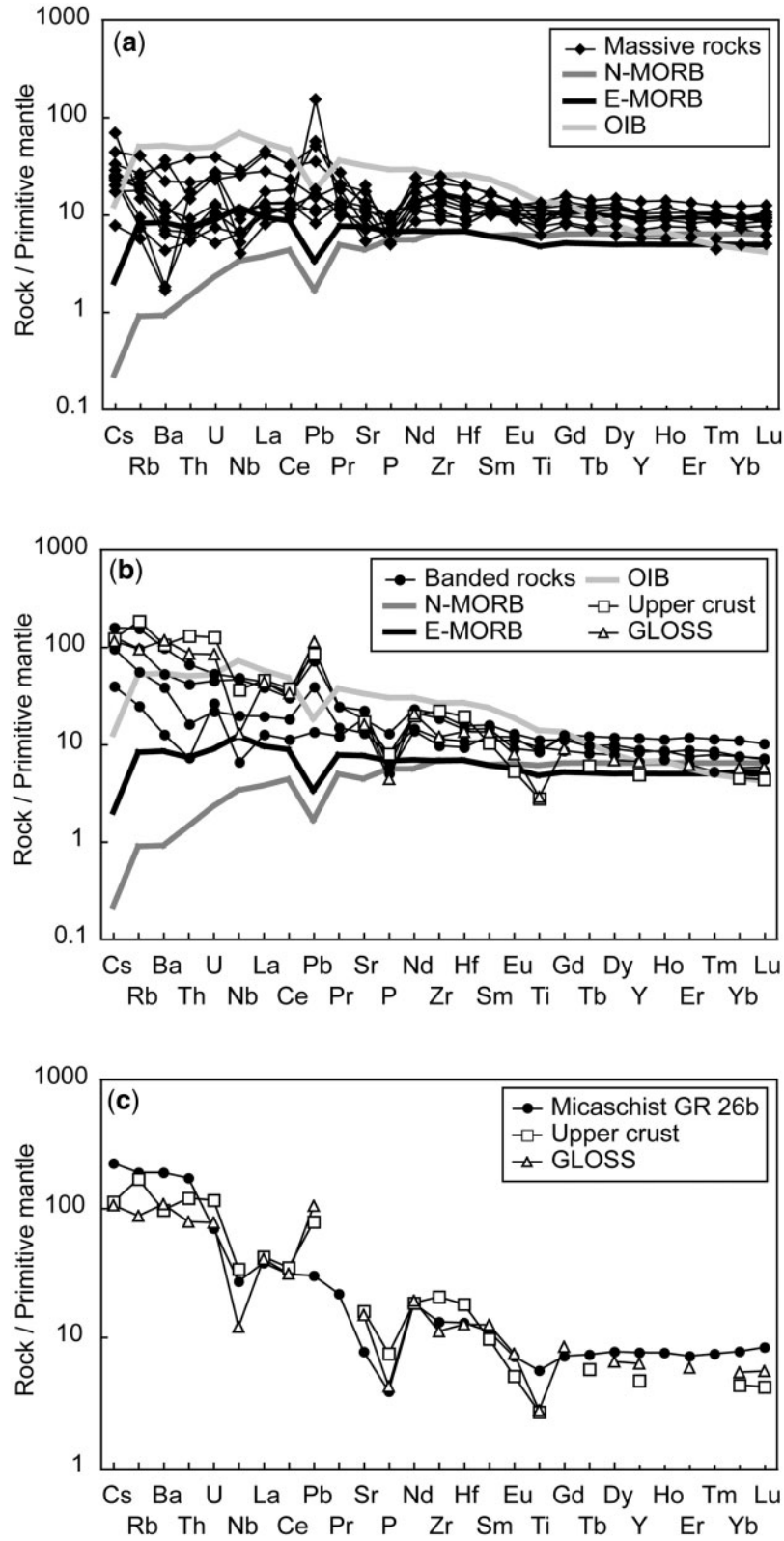


Fig. 5. Primitive mantle-normalized multi-element diagrams illustrating the whole-rock trace element compositions of metabasites (massive and banded rocks) and micaschist GR 26b in comparison with N-MORB, E-MORB, OIB (Sun & McDonough, 1989), upper crust (Taylor & McLennan, 1981) and GLOSS (Plank & Langmuir, 1998). Normalization values are from Sun & McDonough (1989).

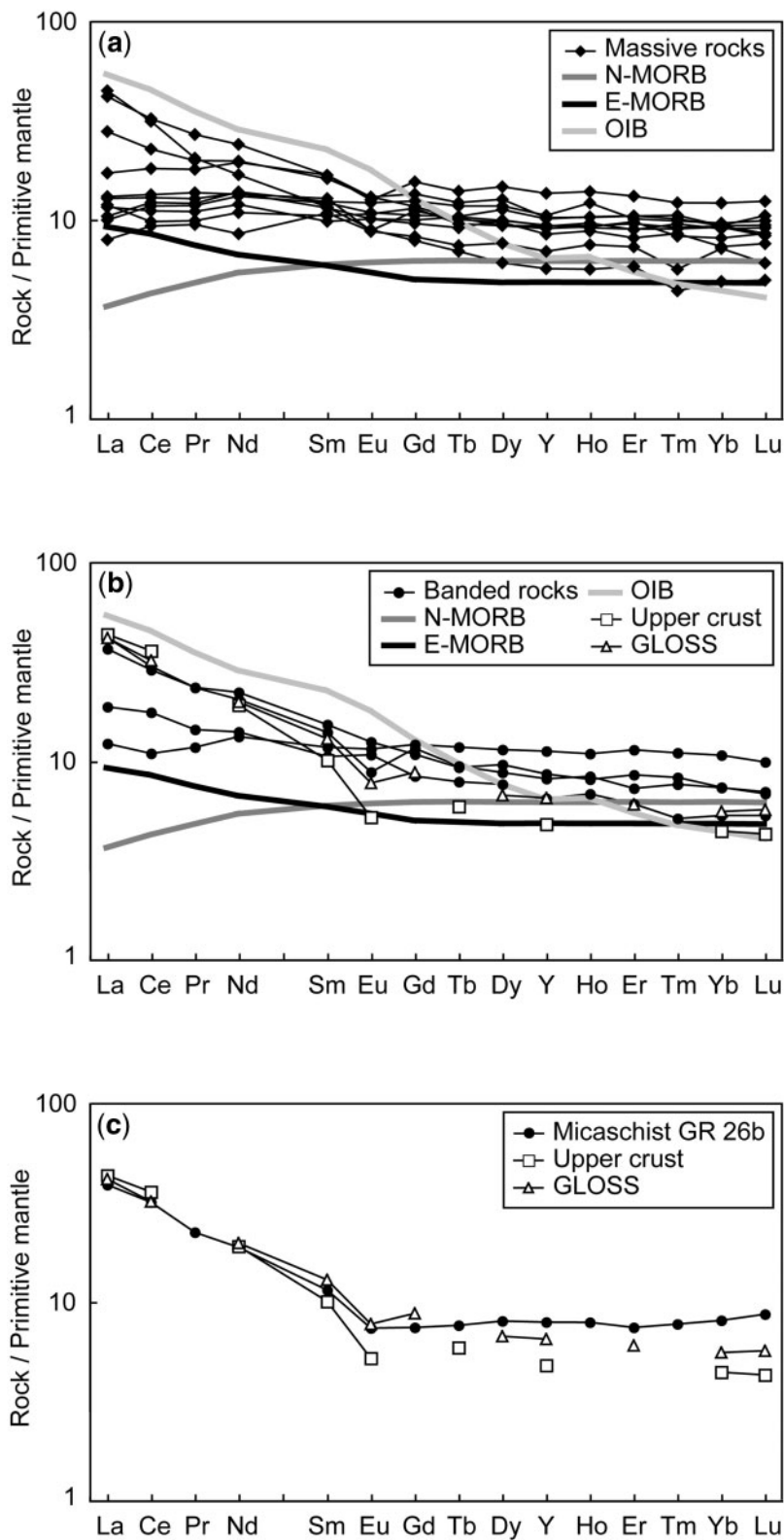


Fig. 6. Primitive mantle-normalized REE patterns of whole-rock metabasites (massive and banded rocks) and micaschist GR 26b in comparison with N-MORB, E-MORB, OIB (Sun & McDonough, 1989), upper crust (Taylor & McLennan, 1981) and GLOSS (Plank & Langmuir, 1998). Normalization values as in Fig. 5.

Table 3. Continued

	Eclogite		Eclogite		Massive BS		Massive GS		Banded BS		MS		Eclogite		Massive GS		Banded BS		MS		Eclogite		Eclogite	
	GR 24a	GR 29	GR 29	GR 29	GR 02	GR 25b	GR 12a	GR 26b	GR 26b	GR 26b	GR 26b	GR 26b	GR 26b	GR 29	GR 02	GR 25b	GR 28	GR 28	GR 26b	GR 26b	GR 24a	GR 29	GR 29	GR 29
	Grt	Grt	Grt	Grt	Grt	Grt	Grt	Grt	Grt	Grt	Grt	Grt	Grt	Grt	Grt	Grt	Grt	Grt	Grt	Grt	Grt	Grt	Grt	Grt
	Core	Rim	Core	Rim	Core	Rim	Core	Rim	Core	Rim	Core	Rim	Core	Rim	Core	Rim	Core	Rim	Core	Rim	Core	Rim	Core	Rim
SiO ₂	37.15	37.36	37.15	37.70	36.87	37.56	37.68	36.42	36.64	36.43	36.79	0.03	0.10	0.03	0.10	0.03	0.15	0.02	0.02	0.02	55.41	55.07	55.07	55.07
TiO ₂	0.13	0.12	0.15	0.06	0.12	0.05	0.11	0.13	0.07	0.09	0.07	n.d.	n.d.	n.d.	0.01	0.01	0.04	0.06	0.06	0.06	0.01	0.03	0.03	0.03
Al ₂ O ₃	21.03	21.15	20.09	20.67	20.34	20.38	21.19	19.36	19.90	20.81	21.36	0.01	0.01	0.01	n.d.	n.d.	0.03	0.01	0.01	0.01	8.77	9.76	9.76	9.76
Fe ₂ O ₃ †	—	—	—	—	—	—	—	—	—	—	—	—	—	—	—	—	—	—	—	—	4.18	6.69	6.69	6.69
FeO†	30.31	28.67	27.88	28.81	29.64	28.75	28.83	21.37	31.98	25.10	27.87	0.05	0.07	0.05	0.07	0.10	0.10	0.09	0.09	3.70	3.10	3.10	3.10	
MnO	1.68	0.41	2.73	0.51	1.54	1.24	0.81	14.45	1.62	8.62	4.22	0.01	0.04	0.01	0.04	0.05	0.01	0.09	0.09	n.d.	0.05	0.05	0.05	
MgO	1.29	1.61	1.36	1.89	1.58	1.88	2.20	0.50	1.09	0.82	0.67	n.d.	n.d.	n.d.	n.d.	n.d.	0.01	n.d.	n.d.	8.22	6.06	6.06	6.06	
CaO	9.05	11.31	9.25	10.06	9.17	9.47	9.67	6.82	7.73	7.35	9.25	55.96	55.36	55.96	56.56	54.14	55.72	55.72	55.72	13.64	11.64	11.64	11.64	
Na ₂ O	0.02	0.02	n.a.	n.a.	n.a.	0.01	0.03	0.03	n.a.	n.a.	0.01	0.07	n.d.	0.01	0.01	0.34	0.04	0.04	0.04	6.56	7.98	7.98	7.98	
K ₂ O	0.01	n.d.	n.a.	n.a.	n.a.	0.01	n.d.	n.d.	n.a.	n.d.	n.d.	n.d.	41.96	42.21	41.49	42.29	n.a.	n.a.	n.a.	n.a.	n.a.	n.a.	n.a.	n.a.
P ₂ O ₅	n.a.	n.a.	n.a.	n.a.	n.a.	n.a.	n.a.	n.a.	n.a.	n.a.	n.a.	2.69	2.51	4.58	2.98	n.a.	n.a.	n.a.	n.a.	n.a.	n.a.	n.a.	n.a.	n.a.
F	n.a.	n.a.	n.a.	n.a.	n.a.	n.a.	n.a.	n.a.	n.a.	n.a.	n.a.	0.04	0.04	0.02	0.02	0.02	n.d.	n.a.	n.a.	n.a.	n.a.	n.a.	n.a.	n.a.
Cl	n.a.	n.a.	n.a.	n.a.	n.a.	n.a.	n.a.	n.a.	n.a.	n.a.	n.a.	0.63	0.71	0.72	n.d.	n.d.	n.d.	n.d.	n.d.	n.d.	n.a.	n.a.	n.a.	n.a.
H ₂ O (calc.)	—	—	—	—	—	—	—	—	—	—	—	—	—	—	—	—	—	—	—	—	—	—	—	—
Total	100.66	100.97	98.61	99.70	99.26	99.35	100.49	99.04	99.03	99.23	100.26	100.30	99.99	102.16	99.00	100.57	100.57	100.57	100.57	100.50	100.38	100.38	100.38	
Si	2.971	2.966	3.020	3.013	2.989	3.019	2.977	2.986	2.999	2.971	2.958	0.002	0.008	0.003	0.012	0.002	0.002	0.002	0.002	2.005	2.011	2.011	2.011	
Ti	0.008	0.007	0.009	0.004	0.007	0.003	0.003	0.006	0.005	0.006	0.004	0.000	0.000	0.000	0.003	0.004	0.000	0.003	0.004	0.000	0.001	0.001	0.001	
Al	1.981	1.979	1.925	1.947	1.943	1.93	1.979	1.883	1.92	1.999	2.024	0.001	0.001	0.000	0.003	0.000	0.003	0.000	0.000	0.374	0.420	0.420	0.420	
Fe ³⁺	—	—	—	—	—	—	—	—	—	—	—	—	—	—	—	—	—	—	—	—	—	—	—	—
Fe ²⁺	2.026	1.904	1.896	1.925	2.035	1.933	1.821	1.911	2.189	1.711	1.874	0.003	0.004	0.006	0.006	0.006	0.006	0.006	0.006	0.111	0.093	0.093	0.093	
Mn	0.114	0.027	0.188	0.035	0.186	0.084	0.16	0.054	0.112	0.595	0.288	0.001	0.003	0.003	0.001	0.006	0.001	0.006	0.006	0.000	0.002	0.002	0.002	
Mg	0.154	0.190	0.165	0.225	0.137	0.225	0.192	0.260	0.132	0.099	0.080	0.000	0.000	0.000	0.002	0.000	0.002	0.000	0.000	0.444	0.330	0.330	0.330	
Ca	0.775	0.962	0.805	0.861	0.720	0.816	0.892	0.821	0.678	0.642	0.797	4.695	4.653	4.653	4.521	4.644	4.644	4.644	4.644	0.529	0.455	0.455	0.455	
Na	0.003	0.003	0.000	0.000	0.000	0.002	0.004	0.001	0.000	0.001	0.002	0.010	0.000	0.002	0.051	0.007	0.051	0.007	0.007	0.460	0.565	0.565	0.565	
K	0.001	0.000	0.000	0.000	0.000	0.001	0.000	0.000	0.000	0.000	0.000	0.000	0.000	0.000	0.002	0.002	0.002	0.002	0.002	0.001	0.000	0.000	0.000	
P	—	—	—	—	—	—	—	—	—	—	—	—	—	—	—	—	—	—	—	—	—	—	—	—
F	—	—	—	—	—	—	—	—	—	—	—	—	—	—	—	—	—	—	—	—	—	—	—	—
Cl	—	—	—	—	—	—	—	—	—	—	—	—	—	—	—	—	—	—	—	—	—	—	—	—
OH	—	—	—	—	—	—	—	—	—	—	—	—	—	—	—	—	—	—	—	—	—	—	—	—
Total	8.033	8.039	8.008	8.010	8.018	8.013	8.031	8.019	8.036	8.025	8.027	8.494	8.472	8.473	8.406	8.455	8.455	8.455	8.455	4.036	4.057	4.057	4.057	
O	12	12	12	12	12	12	12	12	12	12	12	12	12	12	12	12	12	12	12	6	6	6	6	
Mg-no.	7.07	9.09	8.00	10.45	6.32	10.44	9.55	11.99	5.70	5.48	4.10	—	—	—	—	—	—	—	—	80.01	77.99	77.99	77.99	
XFe ³⁺	—	—	—	—	—	—	—	—	—	—	—	—	—	—	—	—	—	—	—	—	—	—	—	
Xalm	66.02	61.74	62.07	63.21	66.10	63.20	59.40	62.72	46.84	70.34	61.68	—	—	—	—	—	—	—	—	23.16	30.14	30.14	30.14	
Xsps	3.71	0.89	6.16	1.14	6.03	2.76	5.23	1.78	32.07	3.61	19.53	9.46	—	—	—	—	—	—	—	—	—	—	—	
Xprp	5.02	6.17	5.40	7.38	4.46	7.37	6.27	8.54	4.26	3.26	2.64	—	—	—	—	—	—	—	—	—	—	—	—	
Xgrs	25.26	31.20	26.37	28.27	23.40	26.67	29.10	26.95	19.16	21.79	21.06	—	—	—	—	—	—	—	—	—	—	—	—	
Xagr	—	—	—	—	—	—	—	—	—	—	—	—	—	—	—	—	—	—	—	—	—	—	—	
Xfd	—	—	—	—	—	—	—	—	—	—	—	—	—	—	—	—	—	—	—	—	—	—	—	
Xaug	—	—	—	—	—	—	—	—	—	—	—	—	—	—	—	—	—	—	—	—	—	—	—	

(continued)

Table 3: Continued

	Eclogite Massive		Massive Banded MS		Eclogite Massive Banded		Eclogite Banded Massive		Massive Banded MS		Eclogite Eclogite						
	BS	GR 29	BS	GR 28	BS	GR 28	BS	GR 28	BS	GR 28	BS	GR 24a					
SiO ₂	49.45	50.37	50.05	48.44	50.49	57.08	57.27	46.25	49.25	56.46	26.62	27.87	24.15	66.86	67.61	2.42	1.06
TiO ₂	0.33	0.13	0.18	0.29	0.19	n.d.	0.05	0.07	0.03	n.d.	0.04	0.08	0.01	n.d.	0.04	n.d.	0.06
Al ₂ O ₃	27.08	27.14	29.05	27.69	25.74	8.87	9.48	12.19	6.96	1.75	1.71	19.93	19.56	20.60	19.70	19.89	0.44
Fe ₂ O ₃ §	—	—	—	—	—	5.74	4.00	7.78	8.70	3.14	4.30	—	—	—	—	—	83.16
FeO§	3.54	2.97	3.04	5.32	3.35	9.30	9.93	9.79	10.15	6.46	5.40	21.22	18.85	29.94	0.25	0.06	0.17
MnO	0.02	0.02	0.05	n.d.	0.01	0.12	0.09	0.08	0.41	0.07	0.04	0.18	0.27	0.34	0.01	0.03	0.09
MgO	3.02	3.11	2.57	2.12	3.43	9.22	8.87	10.04	10.49	17.70	18.55	19.27	20.06	12.49	n.d.	n.d.	0.12
CaO	n.d.	0.01	n.d.	n.d.	n.d.	0.45	0.25	8.47	7.24	10.90	11.52	0.03	0.04	0.01	1.20	0.16	0.21
Na ₂ O	0.50	0.30	0.52	0.58	0.07	7.17	7.15	3.41	3.68	0.98	0.90	0.01	0.03	10.94	11.71	11.78	0.04
K ₂ O	10.31	10.47	10.60	10.28	10.70	0.01	0.01	0.38	0.15	0.04	0.05	n.d.	0.04	0.14	0.02	0.03	0.01
P ₂ O ₅	n.a.	n.a.	n.a.	n.a.	n.a.	n.a.	n.a.	n.a.	n.a.	n.a.	n.a.	n.a.	n.a.	n.a.	n.a.	n.a.	n.a.
F	0.18	0.13	0.08	0.22	0.16	0.15	0.27	0.25	0.29	n.a.	0.24	0.22	0.12	0.14	n.a.	n.a.	n.a.
Cl	0.01	0.01	n.d.	n.d.	0.01	0.01	0.01	0.01	0.01	n.a.	0.01	n.d.	n.d.	0.01	n.a.	n.a.	n.a.
H ₂ O (calc.)	4.32	4.38	4.47	4.29	4.33	2.08	2.01	1.94	1.89	2.14	2.03	11.45	11.61	10.91	—	—	—
Total	98.63	98.94	100.57	99.09	98.39	99.56	98.87	99.78	98.25	99.32	100.27	98.87	98.46	98.48	100.29	99.73	86.33
Si	6.718	6.794	6.655	6.613	6.869	7.938	7.998	6.699	7.236	7.915	7.793	5.521	5.725	5.271	2.935	2.988	2.968
Ti	0.033	0.013	0.018	0.029	0.020	0.000	0.005	0.008	0.003	0.000	0.000	0.006	0.013	0.002	0.000	0.000	0.001
Al	4.335	4.313	4.552	4.454	4.127	1.454	1.561	2.081	1.205	0.289	0.281	4.871	4.734	5.241	1.066	1.011	1.029
Fe ³⁺	—	—	—	—	—	1.082	1.159	1.186	1.247	0.758	0.627	—	—	—	—	—	—
Fe ²⁺	0.403	0.335	0.337	0.608	0.381	0.601	0.420	0.848	0.962	0.331	0.450	3.680	3.238	5.463	0.009	0.002	0.006
Mn	0.002	0.002	0.006	0.000	0.001	0.014	0.010	0.01	0.051	0.008	0.005	0.031	0.046	0.063	0.000	0.001	0.002
Mg	0.612	0.626	0.509	0.431	0.695	1.911	1.847	2.168	2.296	3.698	3.844	5.957	6.144	4.064	0.000	0.000	0.013
Ca	0.000	0.001	0.000	0.000	0.000	0.068	0.038	1.314	1.139	1.637	1.716	0.007	0.009	0.003	0.056	0.007	0.005
Na	0.130	0.077	0.134	0.153	0.020	1.932	1.936	0.959	1.048	0.267	0.242	0.001	0.000	0.011	0.931	0.989	1.003
K	1.786	1.801	1.797	1.790	1.857	0.001	0.002	0.07	0.028	0.007	0.009	0.000	0.010	0.039	0.001	0.002	0.003
P	—	—	—	—	—	—	—	—	—	—	—	—	—	—	—	—	—
F	0.076	0.055	0.033	0.095	0.067	0.066	0.119	0.086	0.153	—	0.104	0.147	0.076	0.099	—	—	—
Cl	0.002	0.001	0.000	0.000	0.002	0.000	0.002	0.003	0.024	—	0.002	0.000	0.000	0.003	—	—	—
OH	3.923	3.944	3.967	3.905	3.931	1.993	1.879	1.911	1.824	2.000	1.894	15.853	15.924	15.898	—	—	—
Total	18.020	17.962	18.008	18.078	17.969	16.972	16.875	16.972	17.216	16.911	16.967	36.074	35.919	36.157	4.999	5.001	5.019
O	22	22	22	22	22	23	23	23	23	23	23	28	28	28	8	8	8
Mg-no.	60.30	65.13	60.13	41.50	64.61	76.09	81.47	71.88	70.48	91.79	89.52	61.81	65.49	42.65	—	—	—
XFe ³⁺	—	—	—	—	—	42.65	35.07	42.62	36.3	50.85	69.09	—	—	—	99.74	98.48	—

n.a., not analysed; n.d., not detected; XFe³⁺ = 100 × Fe³⁺ / (Fe³⁺ + Al); Mg-number = 100 × Mg / (Mg + Fe²⁺).

*All iron is assumed to be Fe³⁺.

†Rt was normalized to one cation.

‡In Grt and Ap, all iron was calculated as Fe²⁺; in Omph iron was calculated as Fe²⁺ and Fe³⁺.

§In Phe, Chl and Ab, all iron was calculated as Fe²⁺; in Gln, Cross, Barr, Act and Mt iron was calculated as Fe²⁺ and Fe³⁺.

¶Hm was normalized to two cations; Mt was normalized to three cations.

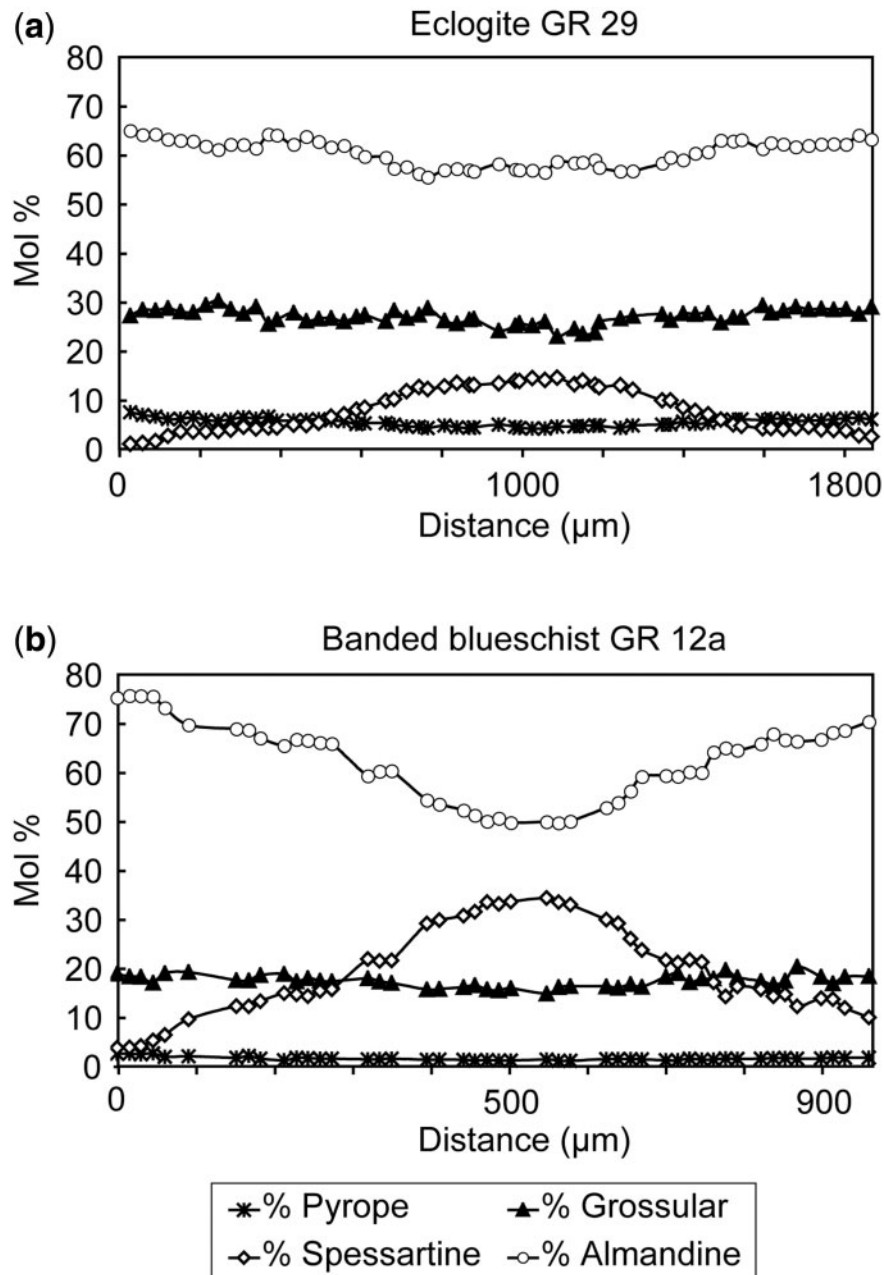


Fig. 7. Chemical zoning of garnet from the massive eclogite GR 29 and the banded blueschist GR 12a. The prograde chemical zoning, defined by the rimward decrease of the spessartine and increase of almandine components, is generally more pronounced in the banded rocks than in the massive rocks.

<http://www.petrology.oxfordjournals.org> (Tables A1–A4 and Tables A5 and A6, respectively).

Eclogites (or omphacite-bearing glaucophanites)

Garnet is strongly enriched in HREE, the concentrations of which are usually higher than those in the whole-rock composition (Fig. 8a and b; Tables 2 and 4). The rimward HREE decrease displays a good correlation with the

major element variations. The trace element composition of epidote shows a large range of variations (Fig. 9a and b). The HREE decrease, whereas the LREE, Th, U and Pb contents increase from epidote I to epidote III (Table 5). Epidote I generally displays a small positive Eu anomaly. The REE, Th, U, Pb and Sr contents of epidote I are similar to those in the whole-rock, whereas they are higher in epidote II and III compared with the

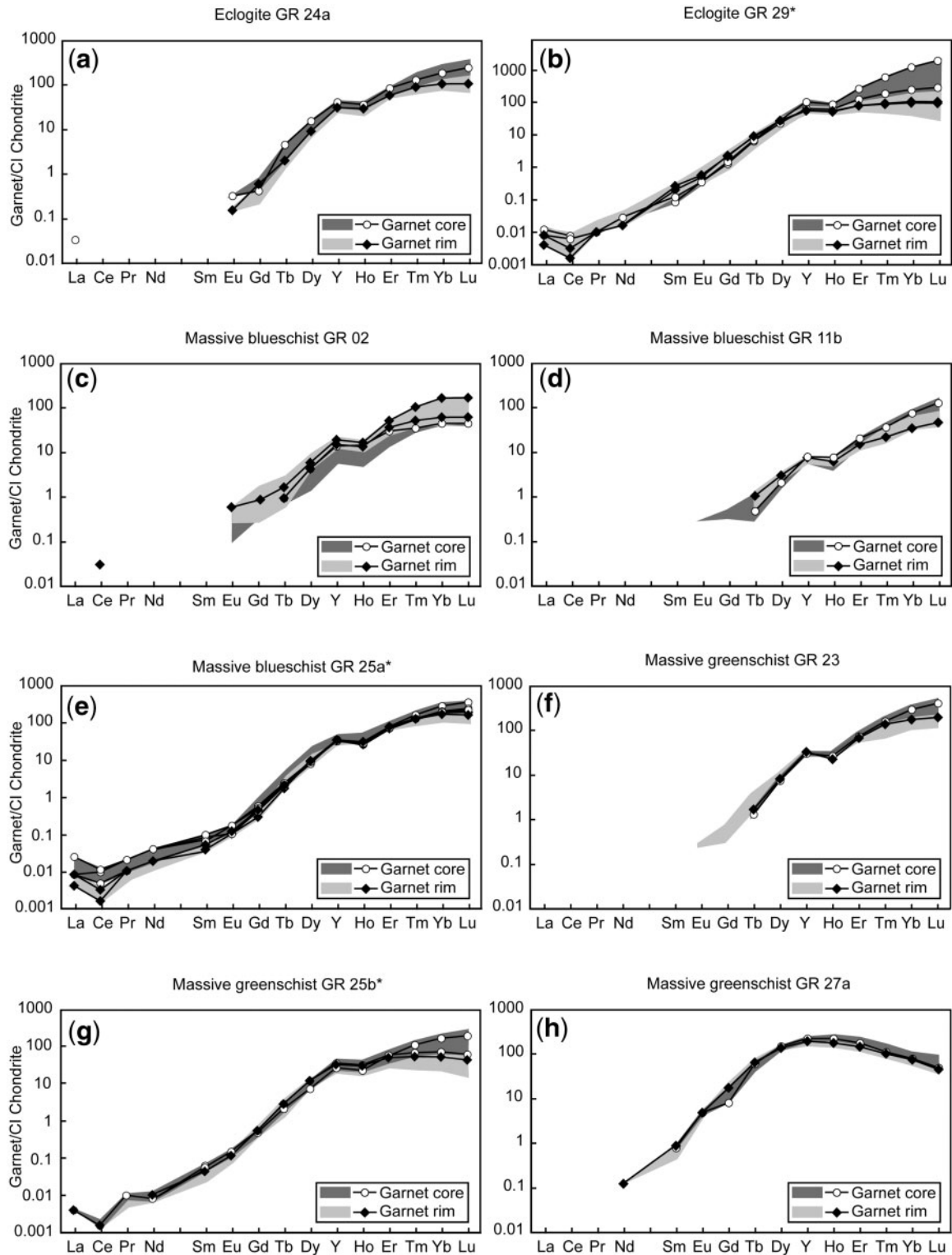


Fig. 8. (a–k) Representative Chondrite-normalized REE patterns for the different generations of garnet in the studied samples. Normalization values as in Fig. 5. *Analyses performed using the Element XR sector field ICPMS.

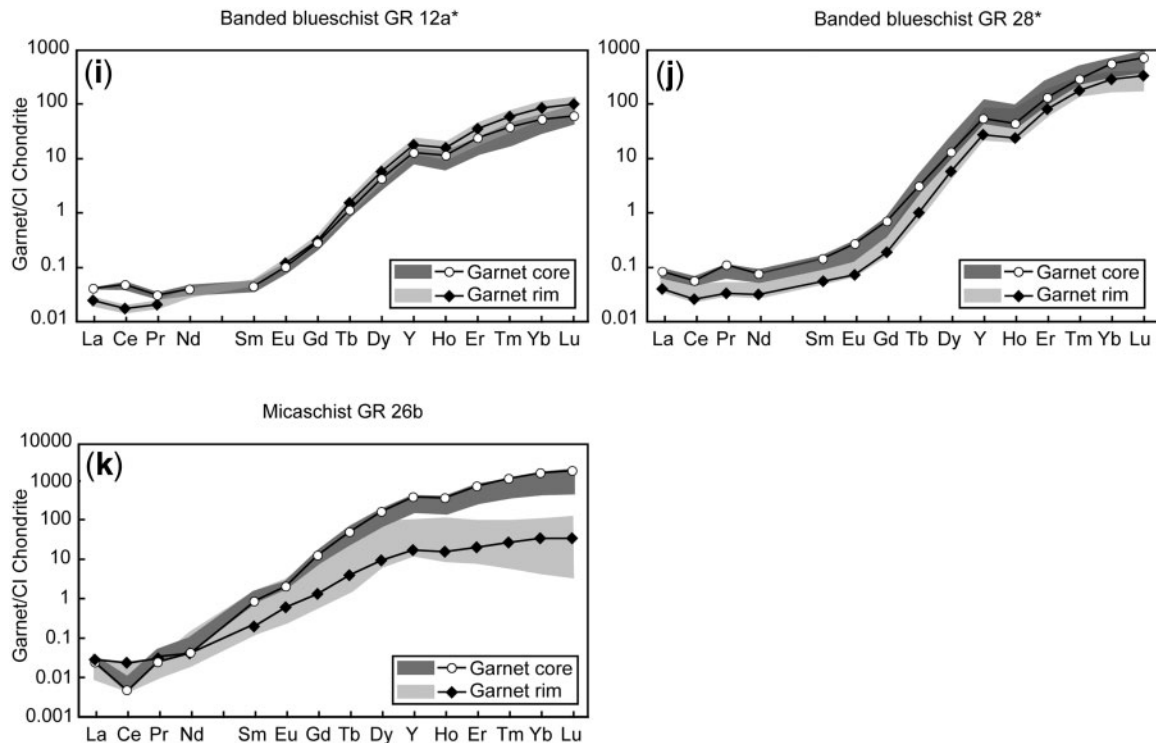


Fig. 8. Continued

whole-rock (Fig. 9a and b; Tables 2 and 5). Phengite is strongly enriched in Cs, Rb, Ba and, to a lesser extent, Sr, Ti, Li and B and mirrors the whole-rock abundances of these elements despite its low modal abundance (Fig. 10; Tables 2 and 6). The Ba content of phengite in sample GR 24a is higher than in GR 29 (4689 and 1154 ppm, respectively), correlating with the whole-rock Ba content of these samples (255 and 12 ppm, respectively). The distribution of Cs and Rb in these samples is similar to that of Ba. In eclogite GR 29, postkinematic phengite (phengite II) is generally LILE depleted compared with the previous generation (phengite I). The major part of the Ti, Nb and Ta budget is trapped in rutile (samples GR 29 and GR 21) and titanite, the latter being HREE enriched (sample GR 24a) (Fig. 11a). Both of these minerals contain small inclusions rich in Zr and Hf that could be zircon. Apatite displays some fractionation of LREE over HREE; the REE are slightly depleted compared with the whole-rock compositions (Tables 2 and 7). It is slightly zoned, with the LREE content decreasing rimwards (Fig. 12a). Barroisite and iron oxides (hematite) contain detectable amounts of HREE (Table 8).

Massive blueschists

Garnet is usually slightly depleted in HREE rimwards, except in blueschist GR 02 (Fig. 8c–e; Table 4), where the HREE slightly increase rimwards. The different

generations of epidote can be distinguished based on the trace element variations (Fig. 9c–e; Table 5): epidote I is LREE depleted, epidote II generally shows only a weak REE fractionation and epidote III is LREE enriched. Phengite is strongly LILE enriched (Fig. 10; Table 6), especially in blueschist GR 12b, mirroring the whole-rock enrichment in LILE. Ti, Ta and Nb are hosted mainly in rutile and titanite (Fig. 11b). Two generations of titanite are sometimes observed: titanite I depleted in HREE and titanite II enriched in HREE. The trace element distribution in apatite varies significantly from sample to sample (Fig. 12b; Table 7), but a LREE enrichment is generally observed (Fig. 12b).

Massive greenschists

Garnet is generally depleted in HREE rimwards and shows the same profiles as garnets from eclogites or blueschists (Fig. 8f–h; Table 4). The four generations of epidote can be distinguished based on their trace element content (Fig. 9f–h; Table 5): prograde epidote I is HREE depleted. The LREE and MREE content increases, whereas the HREE content decreases from epidote I to epidote II. The LREE decrease in retrograde epidote III and IV, which are slightly depleted in trace elements compared with the other generations. Phengite in all greenschists is strongly LILE enriched (Fig. 10; Table 6), but shows a weak depletion in Ba compared with massive eclogites or blueschists

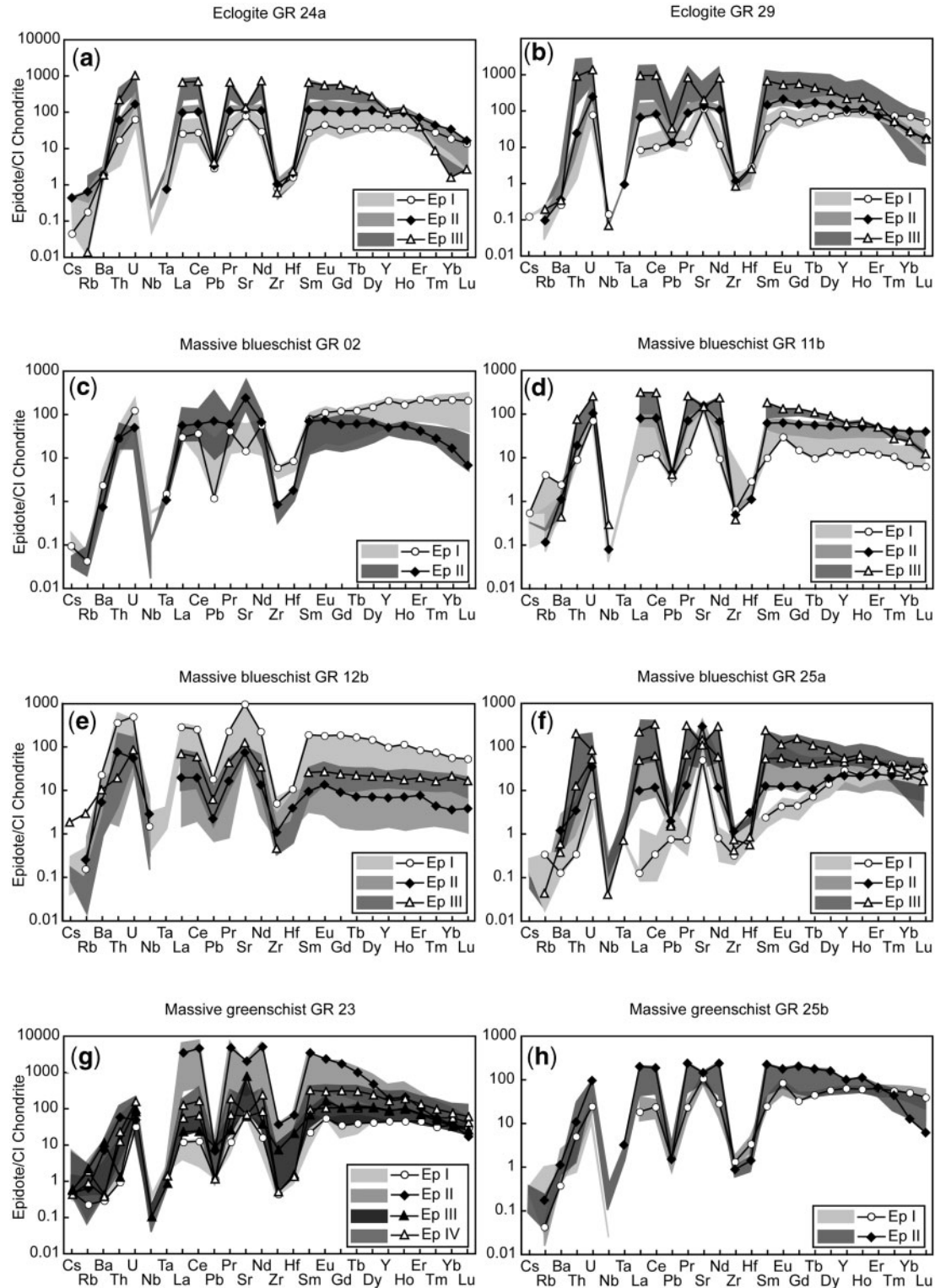


Fig. 9. (a–h) Representative Chondrite-normalized multi-element patterns for the different generations of epidote in the studied samples. Normalization values as in Fig. 5.

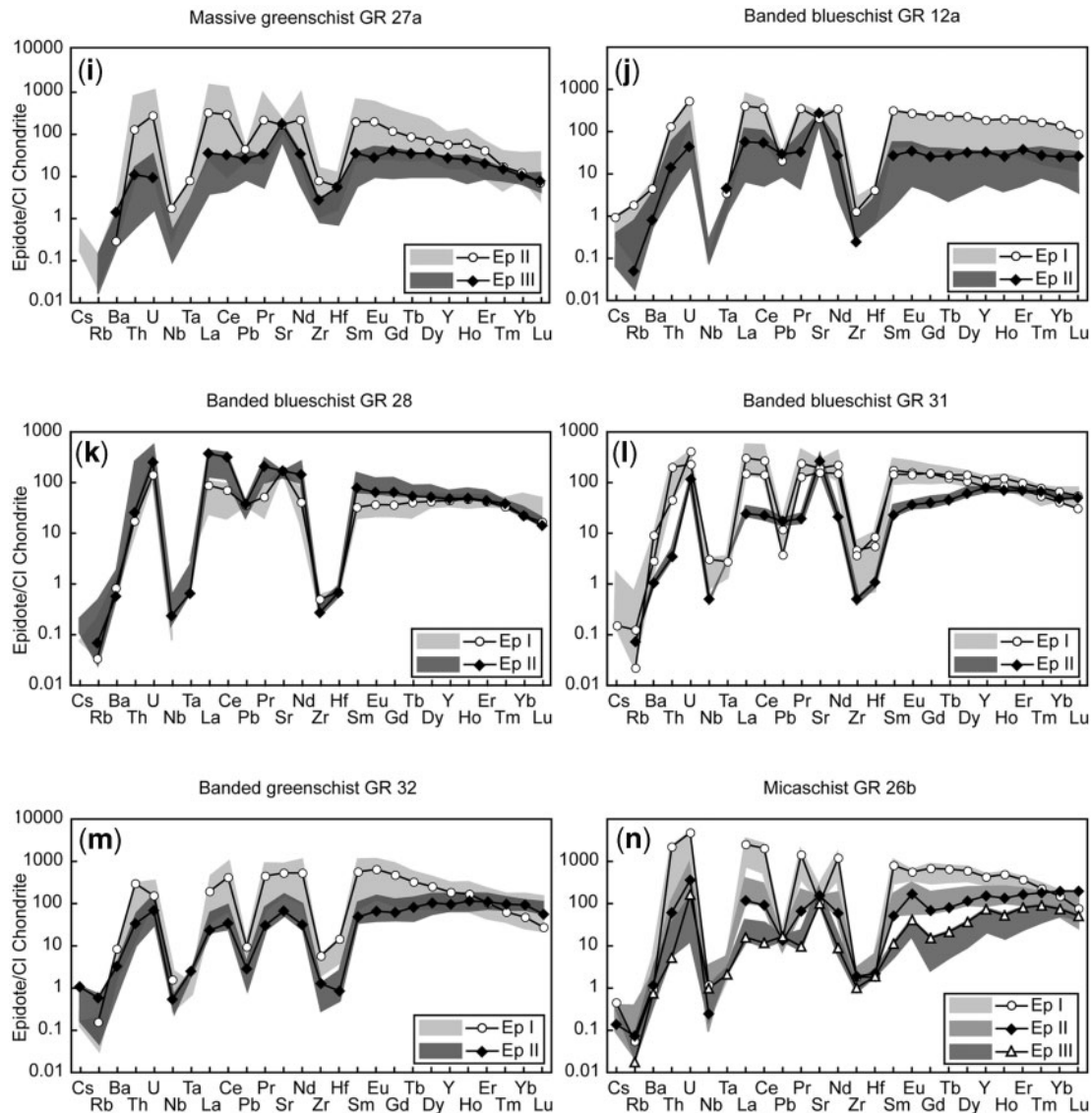


Fig. 9. Continued

in two samples out of three. Phengite in greenschist GR 27a is richer in LILE, reflecting the whole-rock enrichment in LILE (Tables 2 and A6). Titanite and rutile are the main hosts for HFSE (Fig. 11c; Table 7). Two generations of titanite are often present: titanite I depleted in HREE and titanite II enriched in HREE. Apatite is present only in sample GR 25b; it is enriched in LREE (Fig. 12c; Table 7).

Banded blueschists and greenschists

The HREE content in garnet increases rimwards in sample GR 12a (Fig. 8i; Table 4), whereas it decreases in sample GR 28 (Fig. 8j; Table 4). The two epidote generations are generally easily distinguished: epidote I is

enriched in trace elements compared with epidote II in all samples, except GR 28 (Fig. 9j–m; Table 5). Epidote I is usually enriched in LREE compared with HREE and mirrors the whole-rock trace element composition (Fig. 3b). Epidote II is enriched in LREE in sample GR 28 and only shows a weak fractionation of LREE over HREE in sample GR 12a. It is enriched in HREE in samples GR 31 and GR 32. Phengite is strongly LILE enriched (Fig. 10; Table 6). It is richer in Cs, Rb, Ba, Pb and B in samples GR 12a and GR 28 than in samples GR 31 and GR 32, correlating with the differences in the whole-rock compositions (Fig. 5b; Table 2). Titanite is present in all banded rock samples and is strongly enriched in Nb and Ta and HREE (Fig. 11d; Table 7). Accessory rutile (GR

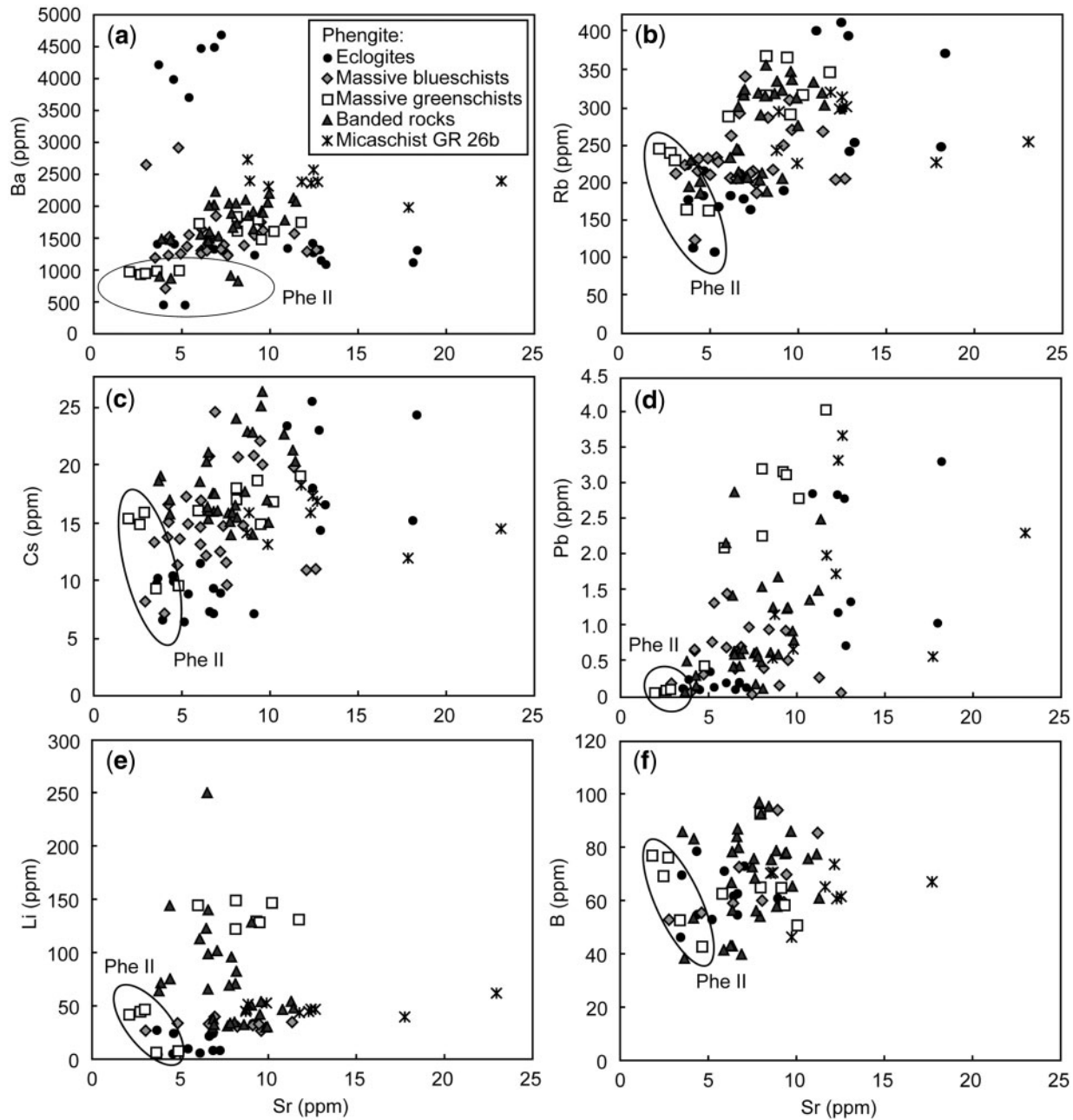


Fig. 10. LILE variations in phengite in the different lithologies. Ellipses indicate the composition of postkinematic phengite II in the massive eclogites, blueschists and greenschists and in the banded rocks.

12a and GR 28) is enriched in Nb and Ta. Apatite is enriched in Sr and REE and shows a fractionation of HREE over LREE, except in sample GR 28 (Fig. 12d; Table 7).

Metapelites

Garnet is zoned in trace elements, displaying a strong rimward HREE depletion (Fig. 8k; Table 4). The three epidote generations are easily recognized (Fig. 9n). Epidote I is

enriched in LREE compared with HREE. Epidote II is depleted in REE and shows no REE fractionation. It displays a positive Eu anomaly. Epidote III is depleted in REE, Th and U compared with epidote I and II (Table 5). It shows MREE depletion and positive Sr and Eu anomalies. Phengite is strongly enriched in Cs, Rb, Ba, and, to a lesser extent, Sr, Ti, Li, B, Nb and Ta (Table 6). Phengite II is LILE depleted compared with phengite I (Fig. 10). Trace element contents in titanite are variable

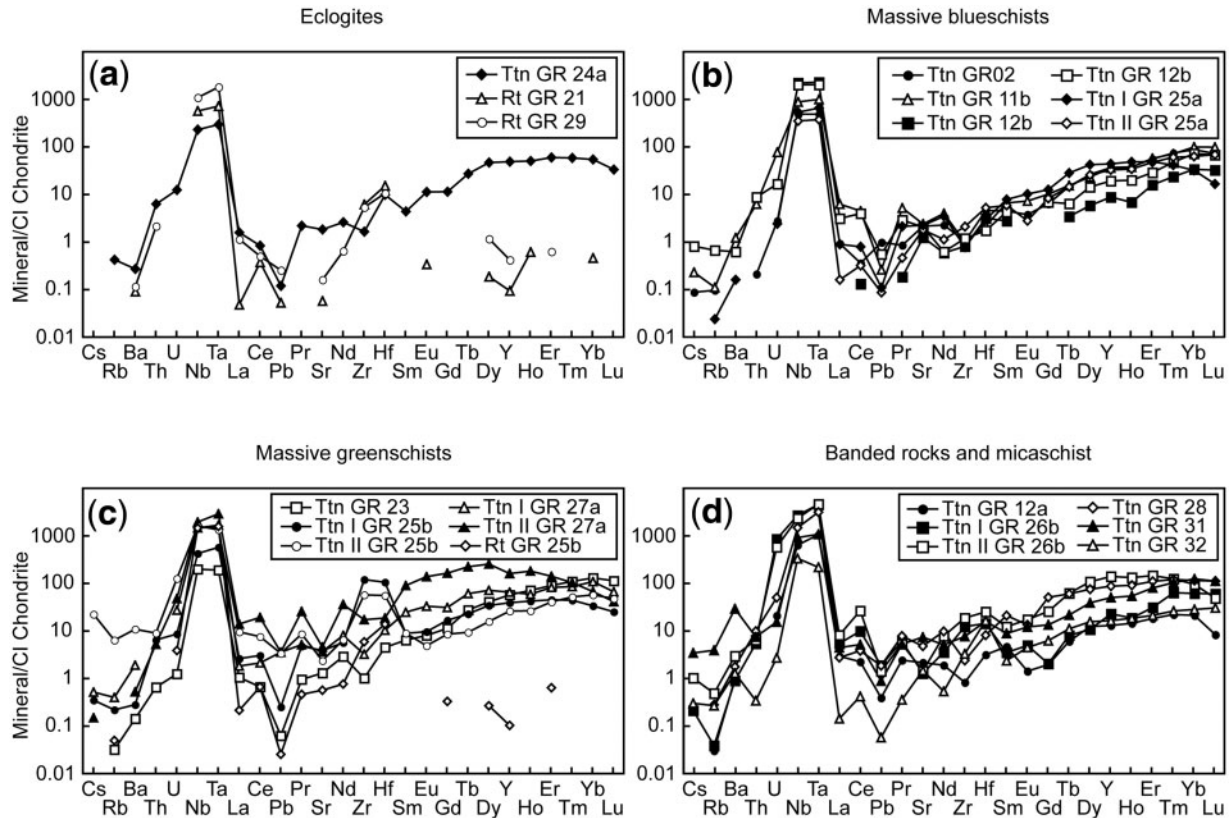


Fig. 11. Chondrite-normalized multi-element patterns for representative analyses of titanite and rutile in each type of rock. Normalization values as in Fig. 5.

(Fig. 11d; Table 7). Two titanite generations are observed, with titanite I being depleted in HREE compared with titanite II (Fig. 11d). Both titanite generations show a slight rimward increase in HREE. Apatite is also zoned in trace elements, with the HREE contents decreasing rimwards (Fig. 12d; Table 7). It displays negative Eu anomalies.

METAMORPHIC *P-T* AND REACTION PATH

A detailed examination of the texture and the chemical zonation of mineral grains such as the garnet porphyroblasts or epidote crystals reveals that they may reflect the *P-T* evolution during their growth, the local chemical environment, and the kinetics of growth. The equilibrium phase diagram of eclogite GR 29 and blueschist GR 02 were modelled using the THERIAK-DOMINO software (de Capitani & Brown, 1987; de Capitani, 1994) to understand the metamorphic reactions controlling the behaviour of trace elements during metamorphism (Fig. 13). A modified internally consistent mineral database based on JUN92 of Berman (1988) modified after Potel *et al.* (2006) was used. The main input consists of the modal bulk

compositions calculated without the minor elements in the system Ti–Ca–NKFMASH. Calculations were performed in the temperature range 350 and 650°C (eclogite GR 29) and 300 and 600°C (blueschist GR 02) and for pressures between 0.5 and 2.5 GPa. In the equilibrium phase diagrams lawsonite is present as a prograde phase, consistent with the observation of totally replaced pseudomorphs after lawsonite.

The peak metamorphic conditions were evaluated at 1.6–2.5 GPa and 550–650°C for the eclogite GR 29 and 1.7–2.3 GPa and 450–525°C for the blueschist GR 02. The pressure conditions are in agreement with those calculated by Bosse *et al.* (2002) for micaschists and Ballèvre *et al.* (2003) for basic rocks. The temperature conditions calculated for the eclogite are higher than those for the blueschist. This difference could be explained by the differences in the parameters used for the calculation, especially water activity. The water activity was fixed at unity for the eclogite to obtain a theoretical peak assemblage corresponding to the peak assemblage of the rock, whereas for the massive blueschist GR 02, a water activity of 0.6 was used, which is more realistic for a subduction zone environment. Considering the geometry of the peak assemblage

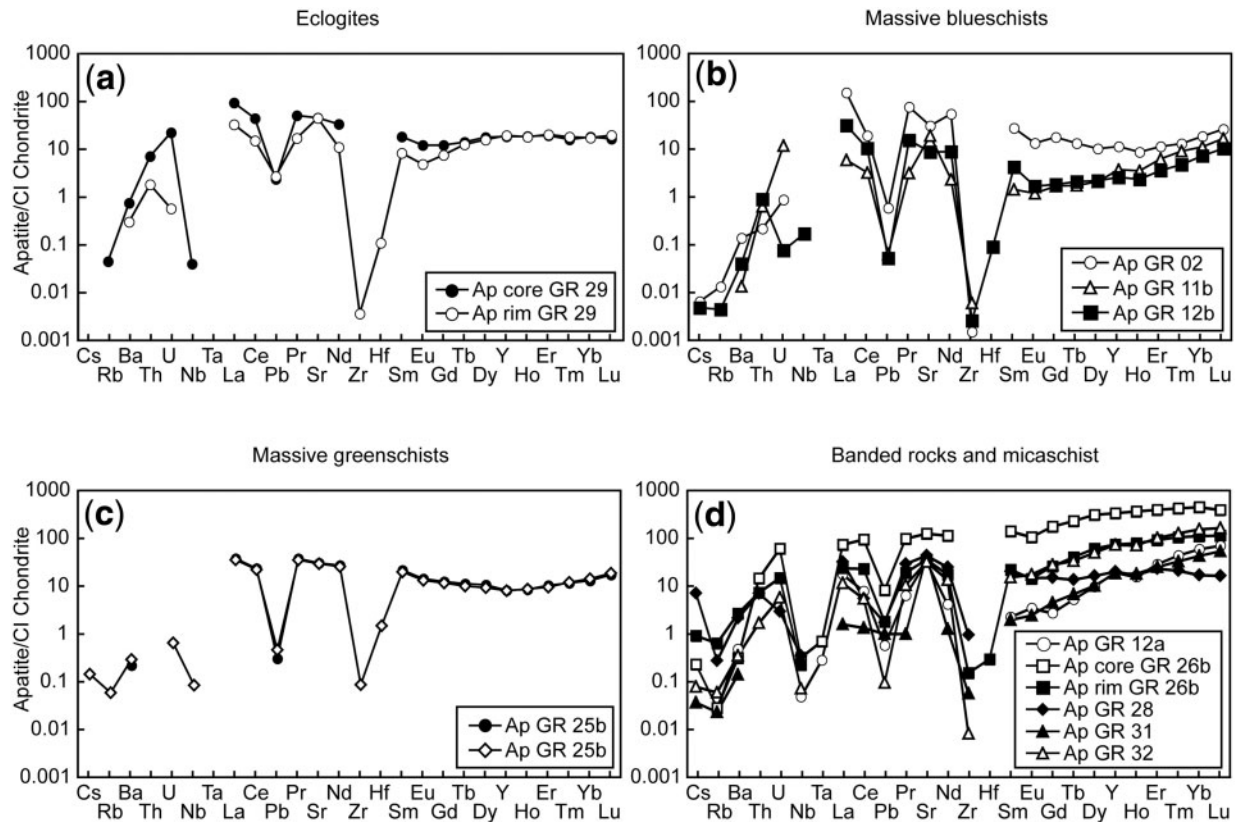


Fig. 12. Chondrite-normalized multi-element patterns for representative analyses of apatite in each type of rock. Normalization values as in Fig. 5.

field, the temperature for eclogite GR 29 may not have exceeded 600°C, as the rock would have passed through the stability field of ilmenite and left the stability field of epidote during the retrograde path. The hematite–magnetite (HM) buffer had to be included for the blueschist GR 02 to take into account the excess of iron in the whole-rock composition, as the rock was oxidized during the late stages of metamorphism. The differences in peak metamorphic conditions also result from the difficulty in modelling the whole assemblage of the rock because of the lack of thermodynamic data for some minerals, especially barroisite.

Eclogite GR 29

For eclogite GR 29, the P – T section indicates a clockwise P – T path (Fig. 13a). The stability fields of rutile, titanite and ilmenite are important markers for the construction of the equilibrium phase diagram. During the prograde path (1.0–2.0 GPa; 350–450°C), early titanite—now preserved as inclusions in garnet—and epidote I crystallized in equilibrium with lawsonite—assumed to have been present in the rock (Fig. 13a). Still in the titanite stability field, a Mn-rich garnet (<6% spessartine) started to crystallize enclosing early titanite. The rock then passed into the

rutile stability field and at peak metamorphic conditions of 1.6–2.5 GPa and 550–650°C, garnet rims (<1% spessartine, <65% almandine) crystallized in equilibrium with omphacite and rutile, present as inclusions in garnet rims, whereas titanite reacted out (Fig. 13a). An early dark blue glaucophane generation was conserved as inclusions in omphacite. Glaucophane grew simultaneously with garnet formation, and along with epidote formed one of the main minerals during the deformation D_1 .

During the retrograde path (Fig. 13a), at P – T conditions lower than 1.6 GPa and 550°C, garnet was partly replaced along its rims by chlorite. Retrograde titanite mantled rutile grains. Phengite remained stable during this part of the P – T path (Fig. 13a). Glaucophane was replaced at the rims by barroisite (Fig. 13a). At the same time, omphacite became unstable and was replaced by symplectites of barroisite and albite.

Blueschist GR 02

During the prograde path (1.1–2.1 GPa; 300–400°C), titanite and epidote I crystallized in equilibrium with lawsonite, of which pseudomorphs are present (Fig. 13b). At higher P – T conditions (1.5–2.3 GPa; 350–450°C), titanite disappeared and was replaced by rutile, whereas

Table 4: Representative trace element compositions of garnet (in µg/g)

	Eclogite GR 24a		Eclogite* GR 29		Massive blueschist GR 02		Massiv blueschist* GR 25a		Massive greenschist* GR 25b		Banded blueschist* GR 12a		Banded blueschist* GR 28		Micaschist GR 26b	
	Core	Rim	Core	Rim	Core	Rim	Core	Rim	Core	Rim	Core	Rim	Core	Rim	Core	Rim
Li	n.a.	<3.6	<2.4	n.a.	0.65	n.a.	<7.0	<9.0	<0.67	<1.7	<4.7	<5.0	1.6	<1.2	3.6	<2.7
Be	n.a.	n.a.	n.a.	n.a.	<1.3	n.a.	n.a.	n.a.	<0.47	<1.1	<1.5	<1.3	<1.6	<1.3	<2.0	<2.3
B	n.a.	n.a.	n.a.	n.a.	13	n.a.	n.a.	n.a.	26	32	10	9.8	12	11	20	15
Sc	128	115	162	60	56	107	109	67	94	109	76	139	123	118	391	147
V	177	133	170	132	63	88	111	101	136	137	18	16	70	63	61	74
Cr	78	46	181	73	152	405	256	281	356	374	422	129	117	224	28	70
Co	0.53	0.64	20	24	n.a.	28	25	25	n.a.	n.a.	n.a.	n.a.	n.a.	n.a.	n.a.	n.a.
Ni	n.a.	<3.9	<2.3	<0.99	<0.39	31	<1.1	2.9	3.4	<0.88	<2.18	<2.2	<1.3	<0.69	4.0	<0.32
Zn	n.a.	21	24	31	23	31	24	23	18	26	25	27	52	48	30	25
Ga	4.4	5.5	n.a.	3.5	2	3.5	3.6	3.8	3.6	3.9	3.1	3.1	4.6	4.8	5.4	5.6
Rb	n.a.	<0.10	0.19	<0.06	<0.02	<0.06	<0.04	<0.06	<0.02	<0.06	<0.02	<0.04	<0.05	<0.03	0.16	0.08
Sr	0.06	0.14	0.03	<0.09	0.03	<0.09	0.06	0.05	0.02	0.02	0.15	0.08	0.47	0.02	0.25	0.03
Y	66	50	186	100	22	31	56	53	57	52	16	35	82	41	702	30
Zr	1.2	0.93	1.5	0.96	0.2	1.5	1.5	0.96	0.98	2.1	0.39	0.33	1.6	1.4	0.31	0.86
Nb	<0.02	<0.02	0.04	0.006	<0.03	0.1	0.12	0.004	0.002	0.002	0.17	0.004	0.99	<0.04	0.008	0.13
Cs	n.a.	<0.07	<0.04	<0.004	<0.004	<0.02	<0.03	<0.03	<0.01	<0.02	<0.02	<0.02	<0.02	<0.02	<0.006	0.02
Ba	n.a.	<0.50	<0.47	<0.19	0.16	<0.19	<0.22	<0.28	<0.04	0.07	0.04	0.04	<0.15	<0.10	0.36	<0.09
La	0.008	<0.009	0.002	<0.02	<0.02	<0.02	0.002	0.002	0.001	0.001	0.01	0.006	0.02	0.009	0.006	0.007
Ce	<0.006	<0.008	0.004	0.02	<0.006	0.02	0.006	0.002	0.001	0.001	0.03	0.01	0.05	0.02	0.003	0.02
Pr	<0.009	<0.003	0.001	<0.05	<0.006	<0.05	0.002	0.001	0.001	<0.001	0.003	0.002	0.01	0.003	0.003	0.003
Nd	<0.07	<0.06	0.01	<0.03	<0.06	<0.03	<0.01	<0.009	0.004	0.005	0.02	<0.008	0.03	0.01	0.02	0.02
Sm	<0.07	<0.03	0.02	<0.04	<0.04	<0.22	0.01	0.008	0.009	0.007	0.007	<0.008	0.02	<0.03	0.14	0.02
Eu	0.02	0.009	0.02	0.03	<0.02	0.04	0.006	0.007	0.009	0.007	0.006	0.007	0.015	0.004	0.13	0.04
Gd	0.09	0.12	0.34	0.52	<0.07	n.d.	0.09	0.09	0.12	0.12	0.06	0.06	0.14	0.04	2.9	0.3
Tb	0.17	0.08	0.29	0.36	0.04	0.06	0.07	0.08	0.11	0.11	0.04	0.06	0.11	0.04	2.1	0.16
Dy	4.0	2.4	8.0	7.5	1.1	1.5	2.0	2.4	3.1	3.1	1.1	1.5	3.21	1.4	48	2.7
Ho	2.1	1.7	5.6	3.3	0.84	0.96	1.5	1.7	1.8	1.7	0.47	1.0	2.4	1.3	24	0.99
Er	14	9.9	50	15	5.1	8.7	13	13	9.9	8.4	4.3	10	21	12	140	3.8
Tm	3.4	2.3	18	2.7	0.91	2.7	4.1	3.2	1.8	1.4	1.6	3.5	7.1	4.3	34	0.77
Yb	33	18	242	21	7.8	29	47	28	12	9.0	20	42	90	46	315	6.5
Lu	6.4	2.8	58	3.0	1.2	4.4	8.9	4.0	1.6	1.1	4.5	7.3	17	8.1	54	0.98
Hf	<0.05	0.03	0.03	0.02	<0.04	0.09	0.02	0.01	0.01	0.62	<0.03	<0.04	0.079	0.21	<0.04	<0.03
Ta	0.01	0.005	0.002	<0.001	<0.01	0.03	0.01	<0.001	0.001	<0.001	<0.01	<0.03	0.05	<0.006	0.01	0.006
Pb	<0.03	<0.02	<0.008	<0.007	<0.03	0.05	<0.01	<0.009	0.009	0.007	<0.05	<0.04	0.04	<0.02	0.61	0.16
Th	<0.02	<0.008	<0.001	<0.001	<0.01	<0.02	0.003	<0.001	0.001	0.001	<0.009	<0.01	0.008	0.005	<0.01	<0.01
U	<0.01	<0.01	0.001	<0.001	<0.005	<0.03	0.004	<0.001	0.001	0.001	<0.009	<0.01	0.007	0.003	0.003	<0.008

*Sr, Y, Zr, Nb, REE, Hf, Ta, Pb, Th and U analysed using the Element XR sector field ICPMS. Henceforth, < values represent analyses below the detection limit.

Table 5: Representative trace element composition of epidote (in $\mu\text{g/g}$)

	Eclogite			Massive blueschist			Massive blueschist			Massive greenschist		Banded blueschist		Micaschist		
	GR 29			GR 02		GR 25a			GR 25b		GR 12a		GR 26b			
	Ep I	Ep II	Ep III	Ep I	Ep II	Ep I	Ep II	Ep III	Ep I	Ep II	Ep I	Ep II	Ep I	Ep II	Ep III	
Li	n.a.	n.a.	n.a.	<2.0	<2.5	n.a.	<1.2	3.9	<2.0	12	<1.1	n.a.	<6.2	<14	<3.1	
Be	n.a.	n.a.	n.a.	<5.0	<4.9	n.a.	n.a.	n.a.	<1.2	<3.2	<2.4	n.a.	<4.0	<4.9	<5.0	
B	n.a.	n.a.	n.a.	47	20	n.a.	13	13	20	36	<5.6	n.a.	33	<50	<14	
Sc	87	96	76	62	96	19	64	322	74	102	193	69	152	353	150	
V	994	1101	823	566	636	801	539	439	830	926	73	142	436	455	423	
Cr	114	196	457	620	840	30	208	59	852	605	470	298	43	118	91	
Co	0.42	0.50	2.1	n.a.	n.a.	0.33	0.51	n.a.	n.a.	n.a.	n.a.	1.5	n.a.	n.a.	n.a.	
Ni	<1.2	1.2	2.5	2.1	<1.4	1.4	<0.72	2.0	6.4	28	2.3	<3.34	9.9	11	0.36	
Zn	3.4	3.5	18	<3.8	5.4	2.0	<1.93	4.5	5.6	21	7.7	<4.35	6.3	14	7.6	
Ga	74	83	94	63	41	43	46	57	55	62	47	43	65	96	82	
Rb	<0.07	0.22	0.45	0.1	<0.07	1.1	<0.06	7.4	0.10	0.41	4.4	0.13	0.17	0.13	0.04	
Sr	811	946	1391	104	951	245	1453	799	794	1074	1470	1948	1146	750	738	
Y	139	166	330	318	65	56	42	416	102	162	289	52	243	684	117	
Zr	4.0	4.5	3.2	23	1.9	1.6	5.6	76	5.2	3.5	5.1	1.0	7.4	7.1	3.9	
Nb	0.04	<0.05	0.02	<0.05	<0.05	<0.04	<0.03	1.0	<0.04	<0.09	<0.03	<0.11	0.06	0.29	0.25	
Cs	0.02	<0.03	<0.02	0.02	0.01	<0.02	<0.03	0.22	<0.02	<0.05	0.18	<0.03	0.03	0.09	<0.01	
Ba	0.62	0.85	0.81	5.7	1.7	0.36	3.4	10	0.93	2.7	11	2.0	2.8	2.3	1.8	
La	2.0	15	214	7.1	10	0.04	3.1	25	4.5	49	93	14	28	609	3.8	
Ce	6.0	48	559	22	31	0.25	8.7	85	15	117	214	33	57	1266	7.3	
Pr	1.3	8.1	76	3.9	5.6	0.08	1.5	12	2.3	23	33	3.2	6.4	139	0.93	
Nd	5.3	48	361	26	31	0.48	6.8	69	14	114	157	13	28	573	4.2	
Sm	5.2	22	99	12	8.9	0.47	2.4	27	3.9	35	47	4.1	7.9	125	1.7	
Eu	4.5	12	29	6.3	3.3	0.35	0.99	15	5.0	11	15	2.0	9.9	33	2.4	
Gd	9.8	31	111	24	11	1.1	3.1	51	6.9	43	48	5.3	14	142	3.2	
Tb	2.4	6.1	16	4.5	2.1	0.34	0.51	9.6	1.7	6.8	8.5	1.0	3.0	25	0.81	
Dy	19	37	87	37	15	4.4	5.9	67	15	41	56	8.2	29	155	9.5	
Ho	5.3	6.2	13	9.4	2.8	1.5	1.5	15	3.5	6.5	11	1.5	7.7	28	3.0	
Er	13	12	22	36	6.5	7.2	4.6	35	11	11	31	6.3	28	62	13	
Tm	1.8	1.2	1.3	5.0	0.61	1.2	0.65	3.8	1.4	1.1	4.2	0.7	4.7	5.9	2.3	
Yb	12	4.2	4.5	36	3.3	6.8	4.4	24	8.8	2.2	24	4.3	34	26	13	
Lu	1.2	0.44	0.42	5.2	0.28	1.1	0.87	3.5	1.0	0.16	2.2	0.66	5.1	2.0	1.3	
Hf	0.31	<0.12	0.26	0.90	0.14	<0.12	0.41	2.3	0.37	0.15	0.45	<0.12	0.24	0.20	0.21	
Ta	<0.03	0.01	<0.03	0.02	n.d.	<0.009	<0.03	0.09	n.d.	0.05	<0.02	0.05	<0.02	<0.09	0.03	
Pb	33	32	79	2.9	59	2.1	5.3	3.8	4.0	3.8	51	73	34	38	42	
Th	<0.03	0.69	25	0.80	1.8	0.007	0.13	0.74	0.15	0.32	3.8	0.41	1.8	65	0.15	
U	0.60	1.9	11	0.97	0.34	0.08	0.35	1.4	0.20	0.79	4.1	0.35	2.9	39	1.3	

epidote I was still stable (Fig. 13b). Around the peak metamorphic conditions (1.7–2.3 GPa; 450–525°C), almandine garnet (<3% spessartine) crystallized in equilibrium with rutile (Fig. 13b), present in the matrix and as inclusions with epidote in garnet. Epidote II formed

simultaneously with garnet during lawsonite destabilization (Fig. 13b).

During the retrograde path, at P – T conditions lower than 1.7–2.1 GPa and 450–500°C, garnet was no longer stable and was partially replaced by chlorite along

Table 6: Representative trace element compositions of phengite (in $\mu\text{g/g}$)

	Eclogite		Massive		Massive		Banded		Micaschist	
	GR 24a	GR 29	BS	BS	GS	BS	BS	BS	GR 26b	
		Phe I*	Phe II	GR 02*	GR 25a*	GR 25b	GR 12a*	GR 28	Phe I	Phe II
Li	7.6	n.a.	n.a.	n.a.	n.a.	5.8	29	47	46	39
Be	4.4	n.a.	n.a.	n.a.	n.a.	4.1	3.9	2.7	<7.0	3.6
B	73	n.a.	n.a.	n.a.	n.a.	53	86	61	61	67
Sc	2.6	4.0	2.0	3.8	4.4	3.1	1.8	3.4	24	12
V	497	396	206	322	384	261	58	226	183	203
Cr	<10	129	15	257	482	226	822	170	100	232
Co	n.a.	12	5.3	20	12	n.a.	n.a.	n.a.	n.a.	n.a.
Ni	6.7	29	18	62	33	21	84	48	92	49
Zn	39	48	20	45	45	25	74	70	112	73
Ga	173	117	41	188	128	62	120	154	107	88
Rb	164	421	113	243	235	163	311	301	312	225
Sr	7.2	13	3.9	7.7	7.5	3.6	9.9	11	12	18
Y	0.28	0.02	0.03	0.05	0.05	<0.03	0.04	<0.04	0.24	0.04
Zr	0.06	<0.10	<0.05	0.86	0.14	3.1	0.04	0.54	3.4	0.12
Nb	0.33	0.08	0.25	0.46	0.49	0.36	0.35	0.29	5.3	17
Cs	8.9	27	6.6	19	13	9.3	17	20	17	12
Ba	4689	1539	459	1896	1456	988	2059	2076	2569	1981
La	0.02	0.02	0.05	0.06	0.02	<0.02	<0.01	<0.01	0.10	<0.01
Ce	<0.02	0.02	0.13	0.09	0.01	0.009	<0.01	<0.03	0.35	0.008
Pr	<0.01	0.004	0.009	0.01	0.006	<0.006	0.009	<0.02	0.02	0.002
Nd	<0.129	0.017	0.12	0.06	0.02	<0.11	<0.11	<0.06	0.19	<0.04
Sm	<0.15	<0.005	<0.10	0.01	<0.01	<0.05	<0.12	<0.07	<0.07	<0.05
Eu	<0.03	<0.002	<0.03	<0.006	<0.003	<0.03	<0.06	<0.03	<0.02	<0.01
Gd	<0.14	<0.01	<0.07	0.02	<0.02	<0.06	<0.07	<0.13	0.07	<0.05
Tb	0.007	0.001	<0.008	0.003	<0.001	<0.008	<0.01	<0.02	0.01	<0.008
Dy	<0.05	0.006	<0.07	0.01	0.02	<0.07	<0.05	<0.07	0.06	<0.03
Ho	<0.02	0.001	0.01	0.002	0.002	<0.01	<0.01	<0.02	0.01	<0.009
Er	<0.06	0.003	0.03	0.004	0.02	<0.03	0.01	<0.03	0.07	0.01
Tm	<0.02	0.001	<0.01	0.002	0.002	<0.01	<0.01	<0.01	<0.007	<0.007
Yb	<0.15	0.003	<0.10	0.01	0.009	0.03	<0.11	0.13	0.15	<0.08
Lu	<0.02	<0.001	0.01	0.001	<0.002	<0.05	<0.01	<0.02	<0.01	<0.008
Hf	<0.4	0.007	<0.03	0.04	0.006	0.29	<0.03	0.10	0.14	<0.04
Ta	0.02	0.007	0.03	0.01	<0.002	<0.02	0.04	<0.05	0.16	0.31
Pb	0.11	2.7	0.23	2.0	0.08	<0.05	0.90	2.5	3.3	0.55
Th	0.008	0.002	<0.02	0.007	0.001	<0.009	<0.01	<0.01	0.03	<0.007
U	<0.01	0.001	0.02	0.006	0.004	<0.008	<0.01	<0.02	0.05	<0.007
Cs/Rb	0.05	0.06	0.06	0.08	0.05	0.06	0.05	0.07	0.05	0.05
Ba/Rb	28.59	3.66	4.06	7.80	6.21	6.06	6.62	6.90	8.23	8.80

*Rb, Sr, Y, Zr, Nb, Cs, Ba, REE, Hf, Ta, Pb, Th and U analysed using the Element XR sector field ICPMS system.

Table 7: Representative trace element compositions of apatite, titanite and rutile (in $\mu\text{g/g}$)

	Eclogite		Massive	Massive	Banded	Micaschist		Eclogite	Massive		Massive	Banded	Micaschist	Eclogite	Massive		
	GR 29	GR 29	BS	GS	BS	GR 26b	GR 26b	GR 24a	blueschist		greenschist	BS	GR 26b	GR 29	GR 25b		
	Ap	Ap	Ap	Ap	Ap	Ap	Ap	Ttn	Ttn I	Ttn II	Ttn I	Ttn II	Ttn	Ttn	Ttn	Rt	Rt
	Core	Rim				Core	Rim										
Li	2.6	<0.46	<0.47	<0.08	13	<3.9	2.8	4.9	<0.68	n.a.	2.9	37	<5.1	<7.8	<4.1	n.a.	<1.64
Be	<0.57	<0.43	<1.3	<0.50	<1.6	<3.0	<3.0	<2.8	<3.1	n.a.	<2.4	<2.3	<1.5	<5.5	<6.2	n.a.	<1.6
B	7.3	7.8	6.6	5.4	13	<19	<7.1	14	12	n.a.	22	20	5.8	<34	23	n.a.	<7.0
Sc	5.8	2.9	6.7	4.3	4.2	<0.80	0.75	2.2	1.5	0.88	4.5	66	1.7	7.1	2.6	1.8	1.6
V	1.7	0.13	1	0.17	3.4	<0.25	1.7	310	428	268	408	1179	60	185	203	1149	1087
Cr	2.4	<1.3	3.7	<1.75	<8.0	<4.9	<2.4	21	69	120	243	970	148	31	64	325	1056
Co	n.a.	n.a.	n.a.	n.a.	n.a.	n.a.	n.a.	n.a.	n.a.	n.a.	n.a.	n.a.	n.a.	n.a.	n.a.	2.2	n.a.
Ni	3.2	0.47	2.9	0.46	18	<0.34	4.4	0.67	<0.42	0.9	8.1	139	<1.7	0.94	1.8	9.2	0.73
Zn	2.4	0.21	<1.4	0.73	13	<0.69	14	36	26	6	17	271	5.6	14	10	28	25
Ga	0.39	<0.10	<0.63	<0.17	2.2	<0.33	0.78	<1.4	<0.83	0.41	2.1	11	1	1	1.1	0.62	<0.40
Rb	0.12	<0.008	0.2	<0.01	0.65	0.07	1.5	0.95	0.05	<0.04	0.51	15	0.07	0.09	1.1	<0.05	0.12
Sr	344	342	407	217	324	937	268	13	16	13	28	17	16	9.3	11	1.1	4.1
Y	30	32	38	12	32	545	119	76	69	51	62	41	21	36	221	0.64	0.16
Zr	<0.03	0.02	0.06	<0.009	3.7	<0.04	0.6	6.2	2.9	8.1	464	222	3.2	48	73	20	23
Nb	0.01	<0.04	<0.02	<0.005	0.09	0.08	0.06	56	134	87	105	399	159	671	583	266	359
Cs	<0.006	<0.004	0.009	0.002	1.4	0.04	0.18	<0.04	<0.02	<0.01	0.07	4.2	<0.02	0.04	0.19	<0.02	<0.02
Ba	2	0.8	1.5	0.51	5.3	0.77	6.5	0.63	0.38	<0.15	0.68	26	2.4	2.2	7.2	0.27	<0.07
La	23	8.2	50	8.7	7.7	18	5.7	0.37	0.21	0.04	0.62	2.3	0.7	1.3	1.9	0.26	0.05
Ce	28	9.8	23	14	3.4	60	14	0.5	0.48	0.19	1.9	4.6	1.4	6.1	16	0.3	0.41
Pr	5	1.7	11.3	3.5	2.8	9.6	1.8	0.2	0.2	0.04	0.45	0.82	0.23	0.58	0.51	<0.05	0.04
Nd	16	5.5	42	12	12	54	8.4	1.2	1.6	0.52	2.6	3.1	0.89	1.7	3.7	0.29	0.36
Sm	3	1.3	7.8	3.2	3.2	22	3.5	0.66	1.2	0.9	1.4	1.4	0.72	0.54	1.9	<0.23	<0.04
Eu	0.74	0.3	1.6	0.81	0.89	6.3	0.85	0.64	0.59	0.16	0.56	0.28	0.08	0.29	1	<0.10	<0.05
Gd	2.7	1.7	7.3	2.5	3.2	37	5.5	2.3	2.6	1.7	3.4	1.8	0.41	0.42	5.3	<0.16	0.07
Tb	0.56	0.5	1	0.41	0.52	8.9	1.6	1	1.1	0.54	0.85	0.35	0.23	0.3	2.3	<0.02	<0.01
Dy	4.7	4.2	5.7	2.6	4.3	81	16	12	11	6.5	8.8	4	3.2	2.7	28	0.29	0.07
Ho	1.1	1.1	1.1	0.47	0.98	21	4.6	2.8	2.7	1.9	2.4	1.5	0.83	1.1	7.6	<0.23	<0.01
Er	3.4	3.5	4	1.7	3.9	68	16	9.8	8.1	7.9	7.5	6.8	3.1	5.2	24	0.1	0.11
Tm	0.43	0.49	0.7	0.29	0.55	11	2.8	1.5	1.1	1.5	1.1	1.3	0.57	1.6	3.2	<0.02	<0.01
Yb	3.2	3.1	6.3	2.2	3	79	19	9.1	5.4	11	5.7	9.7	3.6	11	16	<0.18	<0.12
Lu	0.44	0.52	1.2	0.43	0.43	10	3	0.83	0.42	1.8	0.64	1.2	0.21	1.5	1.3	<0.02	<0.02
Hf	<0.01	0.01	<0.01	<0.02	<0.05	<0.03	0.03	1	0.32	0.55	11	5.9	0.34	1.5	2.7	1.1	1.5
Ta	<0.006	<0.003	<0.02	<0.006	<0.02	0.01	<0.009	4.1	9.4	5.3	8.1	19	15	65	66	25	22
Pb	6.3	7.1	5.1	0.72	4.3	21	4.5	0.29	0.26	0.21	0.62	8.3	0.97	4.7	3.6	0.61	0.06
Th	0.22	0.06	0.03	<0.003	0.21	0.43	0.22	0.18	<0.01	<0.02	0.19	0.26	<0.01	0.16	0.11	0.06	<0.02
U	0.19	0.005	0.02	<0.004	0.02	0.5	0.12	0.1	0.02	<0.02	0.07	1.01	0.17	6.9	4.7	<0.03	0.03

fractures (Fig. 13b). At lower P - T conditions (0.8–1.4 GPa; 300–400°C), retrograde titanite mantled and resorbed rutile (Fig. 13b). Phengite remained stable during this part of the P - T path, as well as chlorite and glaucophane.

During retrogression, barroisite began to crystallize on the rims of glaucophane. Weathering of the rock resulted in the oxidation of chlorite and its replacement by vermiculite.

Table 8: Representative trace element compositions of amphibole, omphacite, chlorite, albite, iron oxides and tourmaline (in µg/g)

	Massive Eclogite		Banded Eclogite		Massive Eclogite		Banded Eclogite		Micaschist		Massive MS		Banded MS		Eclogite		MS	
	BS	GR 29*	BS	GR 24a	BS	GR 25b	BS	GR 31	Chl	Chl	GS	GR 26b	GS	GR 32	Hm	GR 24a	Hm	MS
Act	Gln	Gln	Barr	Omph	Barr	Chl	Chl	Chl	Chl	Chl	Ab	Ab	Mt	Core	Hm	Core	Hm	Tur
Li	n.a.	n.a.	<2.7	116	27	113	46	399	185	157	<2.3	<3.5	<6.4	2.8	4.1	2.1	21	
Be	n.a.	n.a.	7.1	6.8	3.4	3.4	<0.79	0.35	<2.8	<1.5	<1.5	3.4	n.a.	<6.0	1.5	<7.8		
B	n.a.	n.a.	28	11	22	10	21	4.2	77	17	29	26	9.6	85	102	20902		
Sc	53	7.6	61	19	28	n.a.	7.8	2.6	2.4	2.7	<0.71	<0.53	<0.27	<0.78	8.9	3.6		
V	1056	234	647	122	688	n.a.	110	89	77	37	0.69	0.64	312	148	490	157		
Cr	818	141	13	41	<8.6	n.a.	265	274	38	11	<12	<3.3	20	44	42	138		
Co	394	67	n.a.	n.a.	n.a.	n.a.	n.a.	n.a.	n.a.	n.a.	n.a.	n.a.	n.a.	n.a.	n.a.	n.a.	n.a.	
Ni	1505	253	16	148	4.6	n.a.	323	649	394	624	<1.0	<0.42	63	77	115	80		
Zn	857	245	249	233	83	n.a.	418	542	1168	1174	<2.6	0.69	33	18	34	357		
Ga	36	11	13	8.8	15	n.a.	21	25	32	28	7.8	6.2	1.7	<1.9	4.8	22		
Rb	27	0.12	0.3	1.7	<0.03	0.78	0.48	0.59	25	2.2	0.29	0.85	0.71	<0.06	0.22	3.3		
Sr	4.9	0.35	1.3	7.1	3	3.6	2.3	1.2	5.3	1.5	399	16	0.15	24	27	113		
Y	0.25	0.05	0.51	1.2	0.08	0.57	0.03	0.56	0.75	1.4	0.07	<0.01	<0.03	4.7	22	0.14		
Zr	2	1.4	0.16	0.95	0.48	0.91	0.08	0.24	1.9	6.6	<0.08	<0.03	0.13	<0.16	0.22	1.1		
Nb	0.06	0.02	0.03	0.11	<0.02	0.02	<0.02	0.14	1.5	0.25	<0.04	0.02	0.16	<0.06	0.18	<0.04		
Cs	<0.73	n.a.	<0.006	<0.02	<0.009	n.a.	0.02	0.03	1.2	0.2	<0.03	0.04	0.12	<0.03	<0.26	0.36		
Ba	164	0.39	0.13	1.5	1.1	0.05	1.1	0.72	1.3	184	4.7	8.5	0.67	1.9	2.7	1.8		
La	0.06	0.005	<0.01	<0.02	<0.009	0.27	0.02	0.46	0.34	1.6	0.02	<0.009	<0.02	1.5	5.6	0.09		
Ce	0.16	0.008	<0.01	<0.02	<0.01	0.67	0.04	0.9	0.77	3.6	0.07	<0.007	0.14	0.52	2.9	0.09		
Pr	0.02	0.002	<0.006	0.06	<0.01	0.08	<0.01	0.21	0.09	0.45	0.04	<0.01	<0.01	0.42	2.1	0.09		
Nd	0.06	0.007	<0.06	0.29	<0.07	0.35	<0.09	0.55	0.51	1.9	<0.22	<0.09	0.04	2.7	10	<0.20		
Sm	0.02	0.003	<0.01	0.09	0.04	0.11	<0.11	0.18	0.17	0.38	<0.21	<0.04	0.05	0.76	3.1	<0.21		
Eu	<0.008	0.001	<0.01	<0.02	<0.05	0.03	<0.02	0.01	<0.03	0.1	<0.05	<0.01	<0.04	0.14	0.8	<0.05		
Gd	0.02	0.004	<0.05	0.08	<0.12	0.17	<0.07	0.09	0.2	0.49	0.06	<0.06	<0.05	0.82	4	<0.31		
Tb	0.003	0.001	<0.01	0.01	<0.01	0.01	0.01	0.02	0.02	0.06	<0.02	<0.006	<0.009	0.12	0.59	0.02		
Dy	0.06	0.007	<0.03	0.17	<0.03	0.16	<0.03	0.15	0.16	0.31	<0.12	0.01	<0.05	0.66	3.4	<0.11		
Ho	0.01	0.002	<0.01	0.06	<0.009	0.03	<0.007	0.04	0.03	0.06	<0.02	<0.01	0.007	0.19	0.8	<0.03		
Er	0.04	0.008	0.01	0.11	<0.02	0.11	<0.03	0.07	0.11	0.13	<0.09	<0.03	<0.02	0.39	2.4	0.12		
Tm	0.007	0.001	<0.01	0.07	<0.009	0.02	<0.007	0.008	0.009	0.02	<0.02	<0.007	n.d.	<0.04	0.27	<0.03		
Yb	0.04	0.008	<0.05	0.14	<0.06	0.07	<0.11	0.08	0.14	0.21	<0.12	<0.05	0.02	0.31	1.87	<0.20		
Lu	0.008	0.001	<0.02	0.05	<0.009	0.008	<0.01	0.02	0.04	0.05	<0.01	<0.01	<0.01	0.06	0.26	0.04		
Hf	0.09	0.04	0.05	0.14	0.06	0.1	<0.04	0.01	0.14	0.07	<0.12	0.03	<0.04	<0.20	<0.18	<0.15		
Ta	0.004	<0.001	<0.02	<0.03	<0.01	<0.001	<0.02	<0.006	0.02	0.01	<0.03	0.005	n.d.	<0.03	<0.05	0.03		
Pb	1.5	0.06	0.17	0.05	<0.05	0.83	0.02	0.94	3.2	5.3	3.1	0.12	<0.03	0.11	0.9	33		
Th	0.02	0.001	<0.02	0.04	<0.007	0.04	<0.02	0.04	0.1	0.03	<0.02	<0.007	<0.006	<0.02	<0.03	0.04		
U	0.02	0.001	<0.007	0.06	<0.007	0.007	<0.007	0.01	0.24	0.43	<0.02	<0.06	0.02	0.16	0.81	0.04		

*Rb, Sr, Y, Zr, Nb, Cs, Ba, REE, Hf, Ta, Pb, Th and U analysed using the Element XR sector field ICPMS.

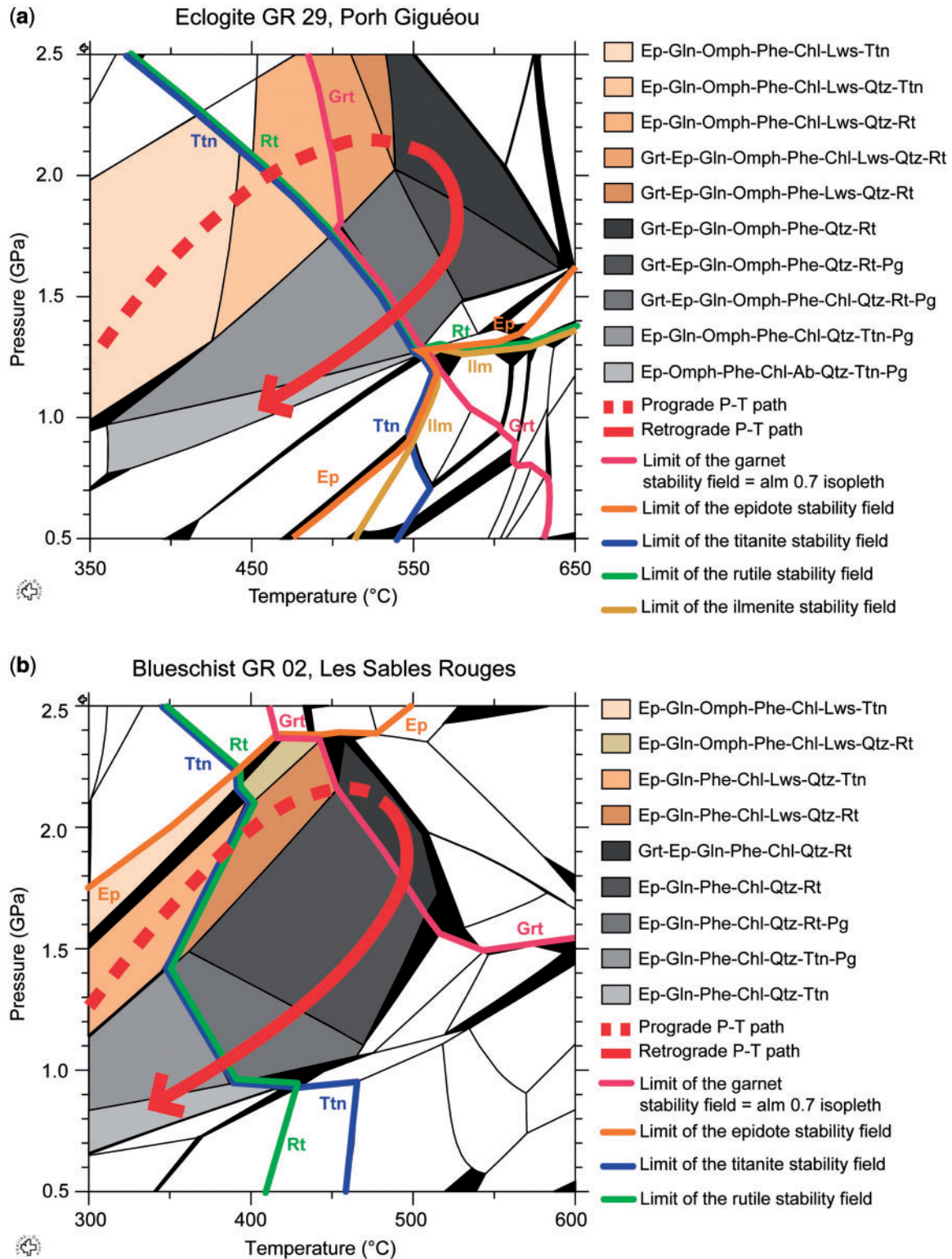


Fig. 13. Pressure–temperature conditions for eclogite GR 29 (a; water activity = 1.0) and massive blueschist GR 02 (b; water activity = 0.6, HM buffer) modelled using the thermodynamic software THERIAK-DOMINO (de Capitani & Brown, 1987; de Capitani, 1994). Omphacite is present in all fields of the diagram for eclogite GR 29. This reflects an excess of an iron-rich calcio-sodic phase (barroisite for example) in the calculated whole-rock composition compared with the actual composition. This results from the difficulty in modelling the whole assemblage of the rock because of the lack of thermodynamic data for some minerals, especially barroisite.

WHOLE-ROCK TRACE ELEMENT BUDGET

Trace element budgets were calculated based on an estimation of the modal proportions of minerals in thin section and their average trace element compositions (Fig. 14). The different generations of epidote and garnet were distinguished to minimize the effect of chemical zonation on calculation uncertainties. Four massive rocks—eclogites GR 24a and GR 29, blueschist GR 25a and greenschist GR 25b—were selected to illustrate the distribution of trace elements at peak metamorphic conditions and during partial retrogression (Fig. 14).

Massive eclogite GR 24a, blueschist GR 25a and greenschist GR 25b trace element abundances were normalized to those in massive eclogite GR 29 and blueschist GR 25a to nearby occurring greenschist GR 25b (Fig. 14a). Despite their different metamorphic facies, the distribution of HREE and HFSE is similar in the four samples. However, the LILE abundances are variable. The Rb, Ba and K contents and, to a lesser extent, Th and U contents, appear to have decreased with retrogression, whereas Sr seems to increase from eclogite GR 24a to greenschist GR 25b.

The distribution of most trace elements is generally well constrained in eclogites with exceptions related to local heterogeneities in mineral composition (phengite, epidote) and to the presence of non-analysed accessory minerals in the rocks (zircon, apatite). Garnet is the main host for HREE. The contribution of garnet core and garnet rims is similar in both eclogites (Fig. 14b and c). Epidote contains more than 95% of the Th, U, Pb, Sr and LREE. Middle REE (MREE) are also preferentially incorporated into epidote. The lack of data for Zr and Hf is linked to the presence of small zircon grains in the matrix and as inclusions in garnet, rutile and titanite (Fig. 14). Epidote III is the main generation hosting REE, Th, U, Pb and Sr. Apatite is only a minor phase for the Sr budget (Fig. 14). Ti and Nb are exclusively incorporated into rutile in eclogite GR 29 (Fig. 14b) and in titanite in eclogite GR 24a (Fig. 14c). Titanite is also enriched in HREE at the expense of garnet. Phengite contains more than 90% of the Cs, Rb and Ba and mirrors the whole-rock composition (Fig. 14b and c). Omphacite, amphibole and iron oxides are negligible in the mass balance.

The distribution of the LILE and REE in the minerals of the blueschist GR 25a and the whole rock budget (Fig. 14d) is comparable to the eclogites (Fig. 14b, c). However, the comparison of blueschist GR 25a (Fig. 14d) to greenschist GR 25b (Fig. 14e) shows differences. Cs, Rb, Th, U, Nb, Pb and LREE show a deficit compared to the whole rock budget. Sr and Ba are present in excess compared to the whole rock budget. Although some elements are additionally incorporated in small quantities in the newly formed retrograde greenschist facies minerals such

as actinolite (Sr, Rb), chlorite (Cs, Rb, Ba) and albite (Cs, Rb, Ba, Pb) the mineral composition cannot be balanced with the whole rock budget. Heterogeneities in the mineral phases and/or a loss of elements during the retrograde metamorphism can be responsible for this poor element budgeting in the greenschist facies sample.

DISCUSSION

Whole-rock geochemistry

The major and trace element patterns of the majority of the massive rocks indicate that they could be derived from MORB-type basaltic protoliths representing subducted oceanic crust (Figs 3 and 4). The relatively high Na and K contents and the LILE and Pb enrichment appear to be caused by seafloor and sub-seafloor hydrothermal alteration during the early stages of metamorphism or by interaction with sediment-derived fluids (Sorensen *et al.*, 1997). Even if Nb presents slight negative anomalies, its content is closed to typical MORB value. Ba negative anomalies in greenschist-facies massive rocks are related to the retrogression process. In eclogite GR 29, the Ba anomaly, as well as the low values of Cs and Rb, reflects the composition of the protolith, which is probably less altered than the other massive rocks. Although the massive samples GR 11b, GR 12b and GR 27a could be interpreted to be of alkali basalt affinity based on their primitive mantle-normalized REE patterns [$(Ce/Yb)_{PM} > 3$], the distribution of HFSE, MREE and HREE is more consistent with MORB-type protoliths (Figs 5 and 6). These samples are restricted to a few small areas of the island (Port St-Nicolas and Les Saisies; see Fig. 1). A larger set of data compared with that used in this study confirms the above observations (El Korh, 2006).

The major and trace element compositions and structural characteristics of the banded rocks suggest that their protoliths could represent a mixture of basic volcanoclastic rocks and continental sediments (Figs 4–6). Compositional variations in the banded rocks could thus be explained by variable sediment contributions to the whole-rock composition. This interpretation is consistent with an increase in the phengite content in the rocks and an increase in Al_2O_3 , K_2O and LILE and decrease in MgO values in the bulk-rocks (Table 2). Based on these characteristics, the contribution of a terrigenous sedimentary component appears to be low in samples GR 31 and 32 and higher in samples GR 12a and 28. The micaschist GR 26b is interpreted as a metapelitic schist derived from a detrital terrigenous sediment similar to GLOSS (Plank & Langmuir, 1998). Its Ti content is higher than that of the upper crust, possibly reflecting the presence of a minor volcanoclastic component. This interpretation is in accord with the previous studies of Bernard-Griffiths *et al.* (1986) and Bosse *et al.* (2002), who concluded that the

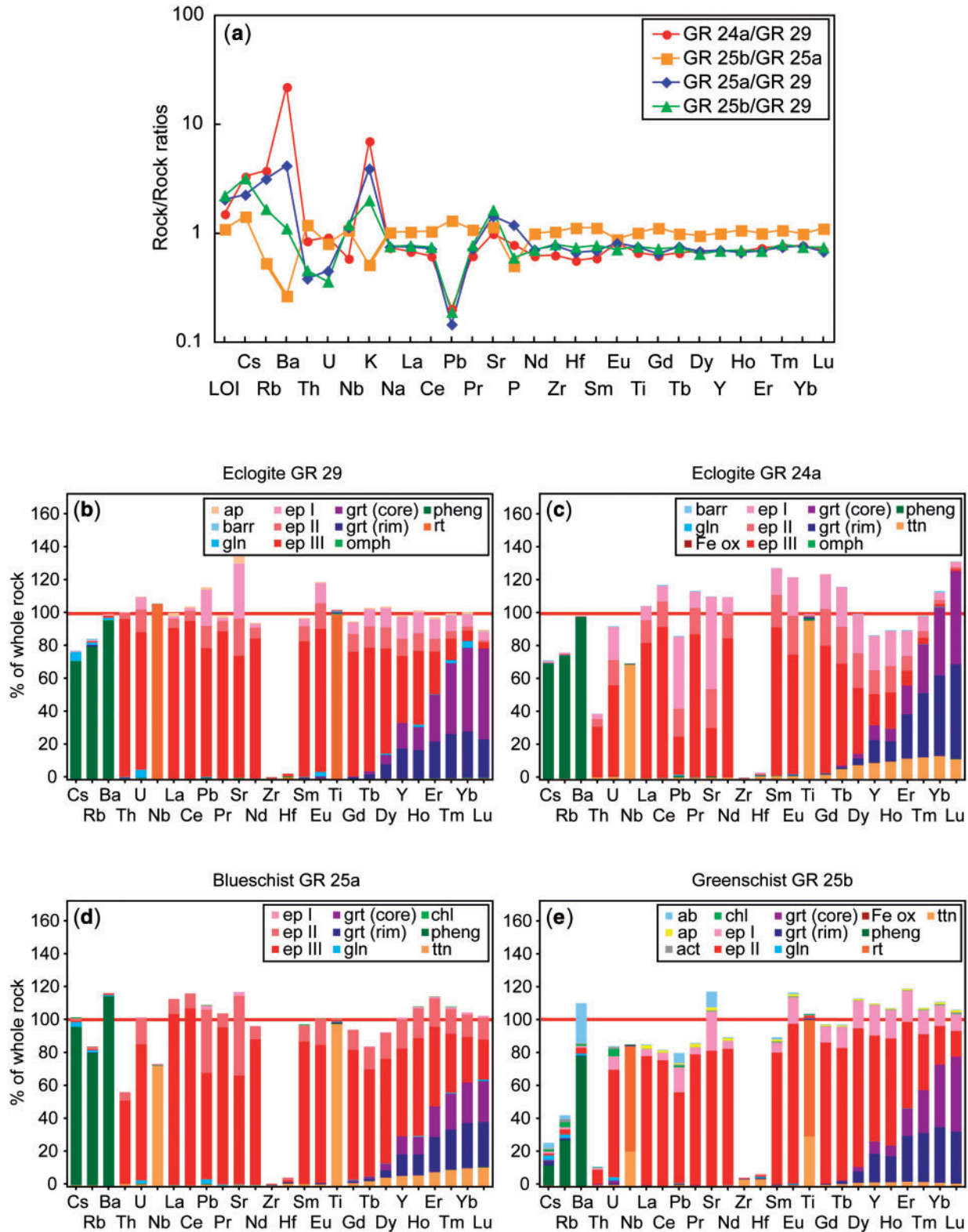


Fig. 14. Comparison of whole-rock composition (a) and mineral-hosted trace element abundances in eclogites GR 29 (b) and GR 24a (c), blueschist GR 25a (d) and greenschist GR 25b (e), compared with those measured in the whole-rock samples. The trace element budget is generally well constrained, except for the LILE. Poor element budgeting is related to heterogeneities in mineral phases or to non-analysed minor minerals.

micaschists of the Ile de Groix are mainly derived from continental sediments.

Trace element distribution in minerals

The trace element abundances in minerals are correlated with the whole-rock compositions and potentially, therefore, with the nature of the protoliths. However, the distribution of incompatible trace elements between the minerals in all of the samples studied is entirely defined by their metamorphic prograde, peak and retrograde assemblages and reaction path, as no pre-metamorphic relicts are contained in them. The main host minerals for incompatible trace elements are lawsonite (LREE, Th, U, Sr, Pb), epidote (REE, Th, U, Pb and Sr), garnet (HREE), phengite (LILE), titanite and rutile (HREE and HFSE).

Lawsonite is not preserved; only pseudomorphs after lawsonite are present. Lawsonite in subduction-related metamorphic rocks is known to be enriched in REE and Sr (\pm Pb, Th and U) (Tribuzio *et al.*, 1996; Spandler *et al.*, 2003; Bebout *et al.*, 2007) and is considered to play an important role in trace element exchange processes. In addition to the Ile de Groix samples, we analysed lawsonite in two blueschist-facies metabasites from the Sesia–Lanzo Zone (Val Orco, Piedmont, Italia) and Haute-Ubaye (France) in the Alps (see Electronic Appendix; Fig. A1). Petrographically and geochemically, these metabasites are comparable with the massive blueschists from this study. Lawsonite in both metabasites is LREE enriched. The degree of the enrichment depends upon its modal abundance and grain size and reaches high values (Lws/CI chondrite *c.* 50–400 and 17–70 for light and heavy REE, respectively). The breakdown of lawsonite can release 3–4% of water and results in the mobilization of trace elements and their redistribution between the newly formed metamorphic minerals (Spandler *et al.*, 2003). Epidote formed after lawsonite shows the same trace element patterns as lawsonite (Fig. A1).

The trace element exchanges in the different mineral assemblages of the studied rocks are discussed below on the basis of rock type (see Electronic Appendix; Fig. A2).

Eclogites

The main compositional feature of garnet is its rimward depletion in the HREE, which appears to be related to the depletion of the rock matrix in these elements during progressive crystallization of garnet, as well as to the accumulation of the HREE in epidote, titanite, and apatite during prograde metamorphism (Fig. 8a and b; Table A1). The slight HREE increase at the core–rim transition in garnet in eclogite GR 24a can be explained by the beginning of lawsonite destabilization after garnet core growth.

The most important phases defining the trace element budget of epidote during metamorphic evolution are lawsonite and garnet. Epidote I is inferred to have crystallized

in equilibrium with lawsonite. The enrichment of epidote II in LREE, Th and U and its depletion in HREE may be connected with the beginning of garnet growth and lawsonite destabilization during metamorphic evolution. Epidote II shows a gradual transition to epidote III. Epidote III is enriched in most incompatible trace elements compared with the previous epidote generations (Table A1), but is depleted in HREE, as it formed in equilibrium with garnet after complete decomposition of lawsonite (see Fig. 9a and b and sections on ‘Petrography’ and ‘Metamorphic *P–T* and reaction path’).

The strong enrichment of phengite in LILE and its depletion in REE, Zr and Hf (Fig. 10) can be explained by the whole-rock composition (rich in K₂O and LILE) and the low abundance of phengite (Tables 2 and 6). The particularly high LILE contents and high Ba/Rb ratios in phengite from eclogite GR 24a seems to be caused by stronger hydrothermal alteration or interaction with a fluid released by the dehydration of the nearby micaschists, enriched in Ba relative to Rb. The partial retrogression resulted in the transfer of Ti, Nb and Ta from rutile (samples GR 29 and 21) to titanite, as well as in the uptake of the HREE from partially chloritized garnet by titanite (GR 24a; see Fig. 11a).

Massive blueschists

The weak HREE depletion rimwards in garnet from most samples can be explained by the depletion of the rock matrix in HREE during the progressive crystallization of garnet as well as by the concomitant crystallization of titanite (Figs 8d, e, and 9d, f; Table A2). An exception is the slight rimward HREE enrichment in garnet from blueschist GR 02, which can be connected with crystallization in equilibrium with rutile and epidote and with the simultaneous destabilization of prograde titanite (Spandler *et al.*, 2003) (Fig. 8c).

The LREE-depleted epidote I, also relatively depleted in trace elements compared with the other generations, probably formed before the crystallization of garnet, in equilibrium with lawsonite, apatite and titanite during the prograde path. Lawsonite pseudomorphs are common in samples GR 11b and 12b (Table 1). The general increase in incompatible trace element contents from epidote I to epidote II can be related to the destabilization of lawsonite during the late stages of the prograde path and with the beginning of garnet crystallization (Fig. 9c–f). Inclusions of epidote in the core zones of garnet show the same trace element pattern as epidote II. Further equilibrium crystallization with garnet constrains the fractionation of LREE over HREE in epidote III (Fig. 9c–f; Table A2).

Prograde titanite I, which is less enriched in Tm, Yb and Lu than retrograde titanite II, may have crystallized in equilibrium with garnet (Fig. 11b). Titanite II formed at the expense of rutile during the weak retrogression and inherited the high Ti, Nb and Ta contents of rutile.

The retrogression resulted in the partial replacement of garnet by chlorite and in the uptake of HREE by titanite II (Table A2). The enrichment of LREE in apatite is related to its formation during the prograde path in equilibrium with epidote (Fig. 12b). Barroisite, chlorite and iron oxides sometimes also demonstrate a moderate enrichment in HREE liberated by the alteration of garnet.

Massive greenschists

Garnet in massive greenschists displays the typical HREE zonation of prograde metamorphism related to the depletion of the rock matrix in the HREE (Fig. 8f–h; Table A3). LREE-depleted epidote I formed in equilibrium with lawsonite before the appearance of garnet. LREE-enriched epidote II crystallized after lawsonite destabilization and accumulated the LREE liberated by this process. The HREE depletion of epidote II indicates that it crystallized in equilibrium with garnet, which is consistent with the textural observations (see the section ‘Petrography’). The depletion of epidote III and IV in LREE compared with epidote II (sample GR 23) seems to be related to the accumulation of the LREE in epidote II and simultaneous depletion of the rest of the system in these elements (Fig. 9g–i; Table A3; compare with the HREE distribution in garnet).

Titanite crystallized during the retrogression, principally in equilibrium with epidote III and chlorite. HREE-depleted titanite I may have formed in equilibrium with garnet during the initial stages of the retrograde path. Titanite II is enriched in HREE, Nb and Ta because of the destabilization of garnet and rutile, respectively (Fig. 11c; Table A3). Small amounts of incompatible trace elements (especially LILE and LREE) were trapped in chlorite, actinolite, iron oxides and albite because of the destabilization of the minerals of the peak assemblage during the retrogression.

Banded blueschists and greenschists

The rimward HREE depletion in garnet from banded blueschist GR 28 follows the typical zonation pattern of prograde metamorphism (Fig. 8j; Table A4). Banded blueschist GR 12a, however, shows HREE enrichment in garnet rims, which can be explained by the partial liberation of the HREE during the replacement of the prograde HREE-rich titanite by rutile (Fig. 8i; see Spandler *et al.*, 2003).

In both samples, epidote I shows a slight fractionation of LREE over HREE (Fig. 9j and k; Table 12). It formed in equilibrium with prograde apatite and titanite. Epidote II in banded blueschist GR 28 crystallized simultaneously with garnet and, therefore, exhibits higher LREE/HREE ratios than epidote I (Fig. 9k; Table A4). Epidote II in banded blueschist GR 12a may have crystallized after garnet during the retrograde path, in equilibrium with retrograde titanite. It became depleted in REE compared

with epidote I, as most of the LREE were still trapped in epidote I, whereas titanite entrained the HREE (Fig. 9j; Table A4).

Depletion of MREE and HREE in apatite rimwards (sample GR 12a) suggests that apatite has grown early during prograde metamorphism in equilibrium with epidote I and was depleted in these elements because of the formation of garnet (Fig. 12d). The destabilization of garnet allowed the transfer of HREE to retrograde titanite and to epidote II in blueschist GR 12a. The destabilization of garnet in blueschist GR 12a resulted in the enrichment of retrograde titanite and epidote II in HREE. The retrograde titanite crystallized in equilibrium with chlorite and barroisite, which trapped small amounts of incompatible trace elements.

In the garnet-free banded blueschist and greenschist rocks (GR 31 and GR 32), epidote is the main host mineral of the REE (Table A4). Epidote I is enriched in LREE (Fig. 9l and m) and may have crystallized in equilibrium with apatite and titanite, both enriched in HREE (Figs 11d and 12d; Table A4). The LREE decrease in epidote II is probably related to the depletion of the crystallization environment in the LREE during the partial retrogression, as epidote I still remains stable and retains significant LREE. Crossite, chlorite, barroisite and magnetite also entrained small amounts of incompatible trace elements during the retrograde metamorphism. The similarity of the trace element contents of epidote, phengite, apatite and titanite in blueschist GR 31 and greenschist GR 32 show that retrogression has a low impact on the trace element budget of these rocks.

The contribution of the terrigenous sedimentary component to the whole-rock composition appears to be an important factor controlling the trace element contents of minerals, especially phengite. In fact, the two groups of banded rocks (GR 12a and 28, GR 31 and 32) have different LILE concentrations, increasing with the amount of the sediment component, and reflected in the LILE compositions of phengite.

Metapelite

The trace element patterns of the minerals, together with textural criteria, allow us to better understand the paragenetic sequence of metapelitic micaschist GR 26b. The LILE contents in phengite mirror the whole-rock LILE composition. Phengite is stable during both the prograde and retrograde paths. The weak LILE depletion of retrograde phengite II compared with phengite I is explained by the depletion of the rock matrix in LILE as a result of their accumulation in phengite I during the early stages of crystallization, as well as by the simultaneous crystallization of retrograde albite. Garnet formed during the prograde path and at peak conditions; it exhibits the typical rimward HREE decrease and constitutes the main host mineral for HREE (Fig. 8k). The strong enrichment in

LREE and depletion in HREE of epidote I can be related to garnet growth during the prograde path (Fig. 9n). Epidote II and epidote III crystallized during the retrograde path and became depleted in LREE, as these elements were trapped in epidote I (see the sections 'Petrography' and 'Mineral chemistry'). Their HREE contents also decreased, because of the growth of retrograde titanite at the time of garnet destabilization (Figs 8k and 11d). The difference in trace element composition of the two generations of titanite can be explained by their formation at different stages of the retrograde path. Apatite, in which the HREE contents decrease rimwards, formed during the retrograde path, probably in equilibrium with epidote II and epidote III, as suggested by the negative Eu anomaly in apatite, which is correlated with the positive Eu anomaly of epidote II and III (Fig. 12d). Biotite and chlorite, which may have formed at the expense of amphibole, and iron oxides inherited a small amount of trace elements during retrogression.

Role of phengite in the LILE trace element budget

The LILE composition of phengite is generally uniform within a sample but varies between samples. Bulk Cs/Rb and Ba/Rb ratios for massive and banded rocks, as well as for metapelite GR 26b, are similar to those of prograde and peak metamorphic phengite (phengite I) from the same lithologies (Tables 2, 6 and A6). These ratios correspond to those of basalts affected by low-temperature alteration (Zack *et al.*, 2001; Miller *et al.*, 2007). However, postkinematic phengite II analysed in eclogite GR 29, blueschist GR 25a, greenschists GR 23 and 25b, and micaschist GR 26b is often LILE depleted. It may have crystallized in equilibrium with retrograde albite, rich in Ba and Sr. Phengite II generally shows the same Cs/Rb and Ba/Rb ratios as phengite I, except in GR 23 and GR 25b. These variations may be related to the retrogression processes (Tables 2, 6 and A6).

Bebout *et al.* (1999, 2007) have observed that Cs and B are mobilized during the dehydration of phengite. No evidence of LILE mobilization during prograde metamorphism was observed during this study. Our results are consistent with those of Zack *et al.* (2001), which have shown that a low fluid–rock ratio is not able to mobilize the LILE content of phengite in eclogites and that the pre-subduction trace element pattern can survive the dehydration process.

John *et al.* (2007) have suggested that an external fluid can interact with a rock and mobilize the LILE and LREE. However, in the case of blueschist GR 25a and especially greenschist GR 25b, the LREE appear to have been mobilized only on a small scale and may not have left the rock, as strong heterogeneities were observed inside each type of mineral, especially epidote, garnet and titanite (Fig. 14a, d and e). Furthermore, the whole-rock

trace element composition of blueschist GR 25a and greenschist GR 25b are similar, except for the LILE, which are depleted in greenschist GR 25b (Fig. 14a). This poor LILE budgeting can be explained by isothermal decompression, which is responsible for the recrystallization and breakdown of phengite (Becker *et al.*, 2000). This implies the partial release of the LILE and their mobilization by interaction with the fluid responsible for the rehydration of the rock (El Korh *et al.*, 2009). Thus, during the greenschist-facies overprint a minor part of the LILE has been re-incorporated into retrograde minerals (especially albite) generating heterogeneities in the rock, and an important part of the LILE is inferred to have escaped from the rocks.

SYNTHESIS

Trace element balance during metamorphism in an intermediate thermal regime subduction zone

The trace element behaviour of mineral assemblages during prograde, peak and retrograde high-pressure metamorphism is summarized in Fig. 15. During the prograde metamorphic path, the main phases able to accumulate large amounts of incompatible elements were lawsonite and, to a lesser extent, epidote I (HREE, Pb, Sr, \pm Th, U), titanite (Ti, Nb, Ta, HREE) and phengite (LILE). Lawsonite formed during prograde subduction-related metamorphism is known to be enriched in REE and Sr (\pm Pb, Th, U) (see the section 'Trace element distribution in minerals' in the Discussion, and references therein) and is responsible for the budget of these elements. The trace element composition of lawsonite in the studied rocks is not known; neither can the amount of incompatible elements released by the destabilization of lawsonite be estimated. It is estimated that 3–4% water leave the rock during lawsonite breakdown (Spandler *et al.*, 2003). Prograde epidote, probably cogenetic with lawsonite—now present as pseudomorphs—is depleted in REE, particularly in the LREE. However, the peak metamorphic epidote is very rich in LREE and Sr. Thus, even if some trace elements have left the system during breakdown of lawsonite and associated fluid escape, a large part of LREE remained trapped in the newly formed mineral phases, especially epidote and, to a lesser extent, titanite and garnet. The positive Eu anomaly commonly observed in epidote I for all rock types is probably related to the breakdown of early plagioclase under increasing P – T conditions (Spandler *et al.*, 2003; Miller *et al.*, 2007). In micaschist GR 26b as well as in massive blueschist GR 12b, the positive Eu anomaly observed in epidote II and III may be related to simultaneous growth with Sr–REE-rich apatite that is relatively depleted in Eu. With increasing P – T conditions, lawsonite and titanite become unstable,

	Prograde path			Peak of metamorphism	Retrograde path
Titanite	Ti, Nb, Ta, HREE	Becomes unstable TE released	TE released to rutile and garnet	—	Ti, Nb, Ta, HREE incorporated
Epidote	Ep I: HREE > LREE Pb, Sr	Ep II: ↑ LREE, Th, U, Pb, Sr ↓ HREE	Ep III: ↑ LREE, Th, U, Pb, Sr ↓ HREE		↓ REE, Th, U, Pb, Sr
Lawsonite	LREE, Th, U, Pb, Sr	Becomes unstable, TE released to Ep II	TE released to Ep III	—	—
Phengite	Cs, Rb, Ba, Sr, Li, B, Be, Ti (with variations within samples)				↓ LILE content, TE released to albite
Apatite	REE, Sr (↓ in the rims)	—			
Glaucophane	Low TE content (excepted Li and B)				—
Garnet	—	Mn-rich garnet (core) ↑ HREE	↓ Mn content ↑ Fe content	Mn-poor garnet (rim) ↓ HREE	HREE released to titanite
Rutile	—	Ti, Nb and Ta			Ti, Nb, Ta released to titanite
Omphacite	—	Low TE content (Li, B, Be, Sr)			—
Chlorite	—	—			Low TE content (Li, B)
Barroisite	—	—			Low TE content (Li depleted compared to Gln)
Albite	—	—			Low TE content (B, Ba, Sr)
Actinote	—	—			Low TE content (Li, B)
Magnétite	—	—			Low TE content

Fig. 15. General paragenetic sequence of the basic rocks. The trace element (TE) exchanges between minerals are represented as a function of the prograde, peak metamorphic and retrograde events. Omphacite is present only in eclogite-facies rocks.

whereas Mn-rich garnet begins to crystallize. LREE, Th, U, Pb and Sr are released and incorporated into epidote II. HREE are transferred from titanite to garnet and, to a lesser extent, epidote II. Under peak metamorphic conditions and probably during the breakdown of lawsonite, epidote III crystallizes and incorporates the main part of the whole-rock LREE content. Its HREE content decreases because of the simultaneous growth of Mn-poor garnet. The HREE and Mn contents of garnet decrease rimwards as these elements become progressively less available in the rock. Rutile is stable and becomes enriched in Ti and HFSE, liberated by titanite destabilization.

During the retrograde path, garnet, phengite and rutile are altered to chlorite and titanite. HREE and HFSE are transferred to titanite. Barroisite crystallizes at the expense of glaucophane. Epidote is still stable and continues to crystallize, but its REE, Th, U, Sr contents decrease as these elements have been trapped into earlier epidote generations. Under lower P - T conditions, actinolite, albite and magnetite crystallize; their incompatible trace element contents are low. The retrograde process associated with

exhumation results in important LILE loss as a result of the destabilization of phengite, but otherwise does not appear to significantly change the overall bulk trace element compositions of the studied rocks. Epidote and titanite control the whole-rock HFSE and REE budget during the retrogression.

Thermal and fluid regime of subduction zones

Several studies have been carried out to understand the processes of trace element exchange in different lithologies during the subduction process in the depth range 70–150 km (Shatsky *et al.*, 1990; Schmidt & Poli, 1998; Tribuzio *et al.*, 1996; Bebout *et al.*, 1999, 2007; Zack *et al.*, 2001; Hermann, 2002; Molina & Montero, 2003; Spandler *et al.*, 2003, 2004; John *et al.*, 2004, 2007; Miller *et al.*, 2007; Usui *et al.*, 2007). The transition from blueschist to eclogite is considered as a major metamorphic process producing large amounts of H_2O by the continuous breakdown of hydrous minerals such as lawsonite, chlorite, clinozoisite-epidote and Na-amphibole to an anhydrous garnet

+ omphacite assemblage (Peacock, 1993a). It is generally assumed that the dehydration of blueschists to dry eclogites is responsible for the strong mobilization of trace elements caused by the breakdown of hydrous phases. The thermal regime influences trace element recycling in subduction zones. In cold subduction zones, the transition from blueschist to eclogite occurs at a depth of ~ 100 km, sometimes as much as 150 km (Peacock, 1993a; Liu *et al.*, 1996). In high-temperature subduction regimes, devolatilization takes place at much shallower levels and the rocks undergo stronger depletion of incompatible elements than in cold subduction zone environments (Bebout *et al.*, 1999; Becker *et al.*, 2000).

Warm subduction zones

Based on the study of the metasedimentary rocks of the epidote-blueschist unit of the Catalina Schist (California), Bebout *et al.* (1999, 2007) concluded that in warm subduction zones (e.g. Catalina Schist 0.5–1.2 GPa, 275–750°C; Cascades, 1 GPa, 400°C), devolatilization is enhanced and significant trace element loss is expected at shallow depths, especially for Cs and B. They concluded that the most extensive devolatilization takes place during the prograde P – T path under epidote-blueschist facies ($>350^\circ\text{C}$). Some Cs and B relative to other LILE and Li is suspected to escape under even lawsonite-blueschist-facies conditions.

Intermediate and cold subduction zones

Bebout *et al.* (1999, 2007) demonstrated that in metasedimentary rocks corresponding to cooler subduction zone environments, micas are able to retain a large proportion of the fluid-mobile trace elements. A significant part of the Cs and B, relative to other LILE and Li, is liberated in such environments at depths of ~ 40 km.

The studies of Tribuzio *et al.* (1996) on lawsonite-blueschist-facies metagabbros from Liguria (Western Italy; 1.2–2 GPa, 500°C) and Spandler *et al.* (2003) on low-temperature mafic and pelitic metamorphic rocks from New Caledonia (0.7–2.0 GPa, 250–600°C) emphasized the role of lawsonite and titanite in low-temperature blueschist-facies rocks as important carriers of LREE and HREE, respectively. They have also shown that allanite and clinozoisite–epidote are the main hosts for the LREE in epidote-blueschist- and eclogite-facies rocks, and that most of the HREE in these rocks are retained in garnet. Molina & Montero (2003) demonstrated the role of destabilization of titanite in the REE and Sr enrichment of epidote during eclogite-facies metamorphism of E-MORB protoliths of the Nevado-Filábride complex (SE Spain; 1.2–2.5 GPa, 500–600°C).

Based on thermodynamic analysis of mineral equilibria, we have determined the peak metamorphic conditions for the studied rocks from Ile de Groix at 1.6–2.5 GPa, 450–600°C, which compares with the estimates for other

HP–LT terranes such as those in Liguria (Tribuzio *et al.*, 1996) and New Caledonia (Spandler *et al.*, 2003). Such estimates correspond to a subduction zone with an intermediate thermal regime (Liu *et al.*, 1996). The blueschist–eclogite transition is estimated to have taken place at $c. 60$ – 70 km. Spandler *et al.* (2003) have shown that under such conditions fluid and trace element release are decoupled during subduction-related dehydration and that the trace elements are redistributed between the different phases of the mineral assemblages. Similarly, Molina & Montero (2003) have argued that the trace element mobilization associated with the continuous breakdown and crystallization of metamorphic minerals under epidote–eclogite-facies conditions is limited to the development of strong trace element zonation of mineral grains. Moreover, the data of Miller *et al.* (2007) on metagabbros corresponding to a ‘warmer’ subduction environment (eclogite facies; 2.2–2.5 GPa, 700–750°C) from Koralpe, Saualpe, Pohorje (Austrian Alps) indicate the same decoupling between fluids and trace elements.

The role of the P – T regime in the mobilization of trace elements during subduction is also evident for ultrahigh-pressure (UHP) metamorphic rocks. The study of Usui *et al.* (2007) on relatively low-temperature UHP metabasaltic rocks from the Colorado Plateau (3 GPa, 560–700°C and 5 GPa, 600–760°C) has demonstrated that the LREE content of lawsonite increases with pressure. This is explained by the destabilization of LREE-rich allanite with increasing pressure. Thus, it is inferred that REE and Sr can be retained in eclogites even in the coesite stability field, provided the slab is cold enough to pass through the lawsonite eclogite facies. Based on observations on alkaline mafic rocks from the Dora Maira Massif (4 GPa, 730°C; Western Alps), Hermann (2002) demonstrated the important role of allanite and other accessory minerals in the LREE and HFSE budget of UHP rocks, and the ability of residual allanite and phengite to control the composition of the subduction zone fluid. Because allanite is stable up to 900–1000°C, the trace elements are retained in the rocks and the formation of a high-temperature hydrous granitic melt must be invoked to explain the mobility of the LREE.

Our data for the subduction-related rocks of the Ile de Groix appear consistent with the interpretations of the above researchers and imply that the subducting oceanic crust experiences only a weak loss of trace elements during high-pressure metamorphism in subduction zones to depths of 50–70 km. We emphasize the role of epidote as an important host of the REE, Sr, Th and U as a result of its large stability field, and its ability to exchange trace elements with lawsonite, titanite and garnet at different stages of the prograde and retrograde metamorphic path during the subduction and exhumation of the studied metamorphic rocks.

Significance of external fluids

Spandler *et al.* (2003) suggested that the mobilization of trace elements from the subducting slab cannot be explained only by the breakdown of minerals, but requires complex fluid–rock interactions. John *et al.* (2007) presented results from Tianshan in China (1.8–2.1 GPa, 480–600°C) indicating that infiltration of large amounts of an external fluid into a blueschist-facies rock and its subsequent transformation into an eclogite can mobilize 40–80% of the LILE, REE and HFSE from the host rock. They also argued that trace elements can be mobilized during prograde metamorphism if the precipitation of new mineral phases is hampered during the dissolution of unstable minerals. Zack *et al.* (2001) have shown that a low fluid–rock ratio is not able to liberate and homogenize the LILE in phengite-bearing eclogites (Trescolmen, Central Alps; 2.0 GPa, 650°C) and that the pre-subduction trace element pattern can survive during the dehydration process. A high fluid–rock ratio is necessary to mobilize the LILE. The metabasites cropping out on the Ile de Groix are generally compact and rather impermeable to fluid percolation. The main fluid–rock interaction is evidenced by the presence of veins, corresponding to fluid channels. Thus, only limited fluid–rock interactions are expected in most of the eclogite- and blueschist-facies rocks during the dehydration process. In volcano-sedimentary rocks and micaschists, the fluid–rock ratios may be higher but this cannot be evaluated with any certainty. Therefore, rehydration associated with the greenschist-facies retrogression constitutes the main evidence for higher fluid–rock ratios in the rocks of the Ile de Groix.

CONCLUDING REMARKS

Studies on trace element exchange during prograde metamorphism in subduction zones generally agree that trace elements are redistributed between newly formed minerals under intermediate and cold thermal regimes (Zack *et al.*, 2001; Hermann, 2002; Molina & Montero, 2003; Spandler *et al.*, 2003; Miller *et al.*, 2007; Usui *et al.*, 2007). Most of the studies argue that, under low-temperature conditions, lawsonite, allanite and titanite are the main trace element carriers. At higher temperature conditions, epidote, garnet and rutile are the main host for trace elements. The various studies show that trace element exchange is only slightly dependent on pressure, because lawsonite and allanite are stable up to UHP conditions (Hermann, 2002; Usui *et al.*, 2007). The temperature conditions are very important for devolatilization reactions and LILE release (Bebout *et al.*, 1999, 2007), but less important for the release of the other trace elements (Hermann, 2002; Miller *et al.*, 2007). Fluid–rock interaction appears to be an important process in trace element mobilization during prograde metamorphism (Spandler *et al.*, 2003; John *et al.*, 2007).

The partial eclogitization of the metabasites of the Ile de Groix implies that the P – T conditions of peak metamorphism were not high enough to cause the breakdown of epidote and phengite, which could release significant amounts of LREE and LILE, and that the fluid–rock ratio was low, allowing the conservation of the pre-subduction trace element patterns in the massive metabasites during the dehydration process. Similarly, the metasedimentary rocks could transport a significant proportion of trace elements to a depth of ~70 km (reaching 150 km in cold subduction environments), where significant devolatilization related to the destabilization of phengite occurs at the blueschist–eclogite transition (e.g. Bebout *et al.*, 1999).

Although the exact trace element composition of the pre-metamorphic protoliths cannot be evaluated with any certainty, the similarity of the trace element patterns of MORB to those of the studied massive rocks indicate that the massive rocks may have largely conserved their incompatible trace element contents during prograde devolatilization reactions and thus retained the geochemical signature of the original basic protoliths, including a hydrothermal alteration overprint. During retrogression, most of the incompatible trace elements stayed trapped in the rocks; only the LILE show evidence of some mobilization.

The trace element patterns of the volcano-sedimentary banded rocks and micaschist GR 26b are largely consistent with those of volcanoclastic and pelitic sediments even after high-pressure dehydration and rehydration reactions related to exhumation. Significant amounts of incompatible elements were preserved in these rocks because of the high modal abundance and the large stability range of phengite, epidote, and apatite.

The trace element contents of minerals in the metabasites from the Ile de Groix, in particular REE and HFSE, are controlled by two main factors: (1) the nature of the protolith and its primary trace element content; (2) the stable mineral assemblage, directly related to the appearance or disappearance of the associated phases (epidote, garnet, titanite and rutile) during the metamorphic cycle. The main minerals controlling the whole-rock trace element budget of the studied subduction-related metamorphic rocks are lawsonite, epidote, titanite and phengite during the early stages of prograde metamorphism. During the pre-peak and peak metamorphism, the trace element budget is defined by epidote, garnet, titanite, rutile and phengite.

Our observations suggest that dehydration reactions in the massive metabasites do not necessarily imply a significant simultaneous trace element release, and that the subduction and exhumation processes could still preserve the primary whole-rock trace element patterns inherited from a hydrothermally altered MORB-like protolith.

ACKNOWLEDGEMENTS

Field-work was allowed by the Scientific Committee of the Réserve Naturelle François Le Bail. We would like to thank Michel Ballèvre for introducing us to the geology of the Ile de Groix, and Catherine Robert for her help with the field sampling and hospitality on the island. Thanks also go to Fabio Capponi for providing XRF analyses. Discussions with François Bussy, Othmar Müntener, Urs Schaltegger and Torsten Vennemann at various stages of this study are much appreciated. Constructive and helpful reviews by Carl Spandler and Reiner Klemd significantly helped us to improve the early version of the manuscript. We are grateful to Marjorie Wilson for the editorial handling of the manuscript and her comments. The research was supported by project 20021-113280 of the Swiss National Science Foundation to S.Th.S and Torsten Vennemann (T.V). The sector field LA-ICPMS analytical work was supported by the SNF instrument installation grant Nr. 206021-117405.

SUPPLEMENTARY DATA

Supplementary data for this paper are available at *Journal of Petrology* online.

REFERENCES

- Agard, P., Yamoto, P., Jolivet, L. & Burov, E. (2008). Exhumation of oceanic blueschists and eclogites in subduction zones: Timing and mechanisms. *Earth-Science Reviews*, doi:10.1016/j.earscirev.2008.11.002.
- Audren, C. & Lefort, J. P. (1977). Géologie du plateau continental sud armoricain entre les îles de Glénan et de Noirmoutier. Implications géodynamiques. *Bulletin de la Société Géologique de France* **XIX** (7), 395–404.
- Audren, C. & Triboulet, C. (1984). Métamorphisme et déformation dans la ceinture de haute pression de l'île de Groix Bretagne méridionale. *Bulletin de la Société Géologique et Minéralogique de Bretagne (C)* **16**, 61–70.
- Audren, C. & Triboulet, C. (1993). Les chemins pression-température enregistrés au cours de la formation de plis non cylindriques dans les schistes bleus de l'île de Groix (Bretagne méridionale, France). *Comptes-rendus de l'Académie des Sciences, Série II* **317**, 259–265.
- Audren, C., Triboulet, C., Chauris, L., Lefort, J.-P., Vignerresse, J. L., Audrain, J., Thiéblemont, D., Goyallon, J., Jégouzo, P., Guennoc, P., Augris, C. & Carn, A. (1993). *Notice explicative de la feuille Ile de Groix à 1/25000 (carte géologique)*. Orléans: BRGM.
- Ballèvre, M., Bosse, V. & Gapais, D. (1998). Les schistes bleus de l'île de Groix (Massif armoricain): un paléoprisme d'accrétion. *Réunion des Sciences de la Terre* **XVII**, Brest. Société Géologique de France ed., Paris, 66–67.
- Ballèvre, M., Pitra, P. & Bohn, M. (2003). Lawsonite growth in the epidote blueschists from the Ile de Groix (Armorican massif, France): a potential geobarometer. *Journal of Metamorphic Geology* **21**, 723–735.
- Barrientos, X. (1992). Petrology of coexisting blueschists and greenschists, Ile de Groix, France: implications for preservation of blueschists. PhD thesis, Harvard University, 252 pp.
- Barrientos, X. & Selverstone, J. (1993). Infiltration vs thermal overprinting of epidote blueschists, Ile de Groix, France. *Geology* **21**, 69–72.
- Bebout, G., Ryan, J. G., Leeman, W. P. & Bebout, A. E. (1999). Fractionation of trace elements by subduction-zone metamorphism—effect of convergent-margin thermal evolution. *Earth and Planetary Science Letters* **171**, 63–81.
- Bebout, G., Bebout, A. E. & Graham, C. M. (2007). Cycling of B, Li, and LILE (K, Cs, Rb, Ba, Sr) into subduction zones: SIMS evidence from micas in high-*P/T* metasedimentary rocks. *Chemical Geology* **239**, 284–304.
- Becker, H., Jochum, K. P. & Carlson, R. W. (1999). Constraints from high-pressure veins in eclogites on the composition of hydrous fluids in subduction zones. *Chemical Geology* **160**, 291–308.
- Becker, H., Jochum, K. P. & Carlson, R. W. (2000). Trace element fractionation during dehydration of eclogites from high-pressure terranes and the implications for element fluxes in subduction zones. *Chemical Geology* **163**, 65–99.
- Berman, R. G. (1988). Internally-consistent thermodynamic data for minerals in the system Na₂O–K₂O–CaO–MgO–FeO–Fe₂O₃–Al₂O₃–SiO₂–TiO₂–H₂O–CO₂. *Journal of Petrology* **29**, 445–522.
- Bernard-Griffiths, J., Carpenter, M. S. N., Peucat, J. J. & Jahn, B. M. (1986). Geochemical and isotopic characteristics of blueschist facies rocks from the Ile de Groix, Armorican Massif (northwest France). *Lithos* **19**, 235–253.
- Bosse, V., Ballèvre, M. & Vidal, O. (2002). Ductile thrusting recorded by the garnet isograd from blueschist-facies metapelites of the Ile de Groix, Armorican Massif, France. *Journal of Petrology* **43**, 485–510.
- Bosse, V., Feraud, G., Ballèvre, M., Peucat, J. J. & Corsini, M. (2005). Rb–Sr and ⁴⁰Ar/³⁹Ar ages in blueschists from the Ile de Groix (Armorican Massif, France): Implications for closure mechanisms in isotopic systems. *Chemical Geology* **220**, 21–45.
- Boudier, F. & Nicolas, A. (1976). Interprétation nouvelle des relations entre tectonique et métamorphisme dans l'île de Groix (Bretagne). *Bulletin de la Société Géologique de France* **XVIII**, 135–144.
- Carpenter, M. S. N. (1976). Petrogenetic study of the glaucophane schists and associated rocks from the Ile de Groix, Brittany, France. PhD thesis, Oxford University, 271 pp.
- Cogné, J., Jeannette, D. & Ruhland, M. (1966). L'Ile de Groix: étude structurale d'une série métamorphique à glaucophane en Bretagne méridionale. *Bulletin du Service de la Carte Géologique d'Alsace-Lorraine* **19**, 41–95.
- de Capitani, C. (1994). Gleichgewichts-Phasendiagramme: Theorie und Software. 72. *Jahrestagung der Deutschen Mineralogischen Gesellschaft. Beihefte zum European Journal of Mineralogy* **6**, 1–48.
- de Capitani, C. & Brown, T. H. (1987). The computation of chemical equilibrium in complex systems containing non-ideal solutions. *Geochimica et Cosmochimica Acta* **51**, 2639–2652.
- Djro, S. C., Triboulet, C. & Audren, C. (1989). Les chemins pression-température-temps-déformation-espace (*P–T–t–d–e*) dans les micaschistes associés aux schistes bleus de l'île de Groix, Bretagne Méridionale, France. *Schweizerische Mineralogische und Petrographische Mitteilungen* **69**, 73–90.
- El Korh, A. (2006). Métamorphisme HP–BT dans les metabasites de l'île de Groix, France: étude pétrologique et géochimique. Masters thesis, University of Geneva, 334 pp.
- El Korh, A., Schmidt, S. Th., & Ulianov, A. (2007). Trace element data and fluid regime during HP–LT metamorphism of basic rocks, Ile de Groix, France. Goldschmidt 2007 Abstracts, Cologne. *Geochimica et Cosmochimica Acta* **71** (15), Supplement 1, A254.
- El Korh, A., Schmidt, S. Th. & Ulianov, A. (2009). Effects of retrogression on trace element contents of metabasites, Ile de Groix, France. *Geochimica et Cosmochimica Acta* **73** (13), Supplement 1, A325.
- Gao, J. & Klemd, R. (2001). Primary fluids entrapped at blueschist to eclogite transition: evidence from the Tianshan meta-subduction

- complexes in northwestern China. *Contributions to Mineralogy and Petrology* **142**, 1–14.
- Gao, J. & Klemd, R. (2003). Formation of HP–LT rocks and their tectonic implications in the western Tianshan Orogen, NW China: geochemical and age constraints. *Lithos* **66**, 1–22.
- Hermann, J. (2002). Allanite: thorium and light rare earth element carrier in subducted crust. *Chemical Geology* **192**, 289–306.
- Hermann, J. & Green, D. H. (2001). Experimental constraints on high pressure melting in subducted crust. *Earth and Planetary Science Letters* **188**, 149–168.
- John, T., Scherer, E., Haase, K. M. & Schenk, V. (2004). Trace element fractionation during fluid-induced eclogitization in a subducting slab: trace element and Lu–Hf/Sm–Nd isotope systematics. *Earth and Planetary Science Letters* **227**, 441–456.
- John, T., Klemd, R., Gao, J. & Garge-Schönberg, C. D. (2007). Trace-element mobilization in slabs due to non steady-state fluid–rock interaction: Constraints from an eclogite-facies transport vein in blueschist (Tianshan, China). *Lithos* doi:10.1016/j.lithos.2007.09.005.
- Kerrick, D. M. & Connolly, J. A. D. (2001). Metamorphic devolatilization of subducted oceanic metabasalts: implications for seismicity, arc magmatism and volatile recycling. *Earth and Planetary Science Letters* **189**, 19–29.
- Kirby, S., Engdahl, E. R. & Denlinger, R. (1996). Intermediate depth intraslab earthquakes and arc volcanism as physical expressions of crustal and uppermost mantle metamorphism in subducting slabs. In: Bebout, G., Scholl, D. W., Kirby, S. H. & Platt, J. P. (eds) *Subduction: Top to Bottom. Geophysical Monograph, American Geophysical Union* **96**, 195–214.
- Kretz, R. (1983). Symbols for rock-forming minerals. *American Mineralogist* **68**, 277–279.
- Liu, J., Bohlen, S. R. & Ernst, W. G. (1996). Stability of hydrous phases in subducting oceanic crust. *Earth and Planetary Science Letters* **143**, 161–171.
- Maekawa, H. (1993). Blueschist metamorphism in an active subduction zone. *Nature* **364**, 520–523.
- Miller, C., Zanetti, A., Thöni, M. & Konzett, J. (2007). Eclogitization of gabbroic rocks: Redistribution of trace elements and Zr in rutile thermometry in an Eo-Alpine subduction zone (Eastern Alps). *Chemical Geology* **239**, 96–123.
- Molina, J. F. & Montero, P. (2003). The behaviour of trace elements in high-*P* mineral assemblages: a LA-ICP-MS study of mafic rocks from Nevado-Filábride complex (SE Spain). *Schweizerische Mineralogische und Petrographische Mitteilungen* **83**, 97–109.
- Morris, J. D., Leeman, W. P. & Tera, F. (1990). The subducted components in island arc lavas: constraints from Be isotopes and B–Be systematics. *Nature* **344**, 31–36.
- Peacock, S. M. (1990). Fluid processes in subduction zones. *Science* **248**, 329–337.
- Peacock, S. M. (1993a). The importance of blueschist → eclogite dehydration reactions in subducting oceanic crust. *Geological Society of America Bulletin* **105**, 684–694.
- Peacock, S. M. (1993b). Large-scale hydration of the lithosphere above subducting slabs. *Chemical Geology* **108**, 49–59.
- Peacock, S. M. (2001). Are double seismic zones caused by serpentine dehydration reactions in subducting oceanic mantle? *Geology* **29**, 299–302.
- Pearce, N. J. G., Perkins, W. T., Westgate, J. A., Gorton, M. P., Jackson, S. E., Neal, C. R. & Chenery, S. P. (1997). A compilation of new and published major and trace element data for NIST SRM 610 and NIST SRM 612 glass reference materials. *Geostandards Newsletter* **21**, 115–144.
- Perchuk, A. & Philippot, P. (1997). Rapid cooling and exhumation of eclogitic rocks from the Great Caucasus, Russia. *Journal of Metamorphic Geology* **15**, 299–310.
- Phillipot, P. (1993). Fluid–melt–rock interaction in basic eclogites and coesite-bearing metasediments: Constraints on volatile recycling during subduction. *Chemical Geology* **108**, 93–112.
- Plank, T. & Langmuir, C. H. (1988). An evaluation of the global variations in the chemistry of arc basalts. *Earth and Planetary Science Letters* **90**, 349–370.
- Plank, T. & Langmuir, C. H. (1993). Tracing trace elements from sediment input to volcanic output at subduction zones. *Nature* **362**, 739–742.
- Plank, T. & Langmuir, C. H. (1998). The chemical composition of subducting sediment and its consequences for the crust and mantle. *Chemical Geology* **145**, 325–394.
- Potel, S., Ferreira Mählmann, R., Stern, W. B., Mullis, J. & Frey, M. (2006). Very low-grade metamorphic evolution of pelitic rocks under high-pressure/low-temperature conditions, NW New Caledonia (SW Pacific). *Journal of Petrology* **47**, 991–1015.
- Quinquis, H. (1980). Schistes bleus et déformation progressive: l'exemple de l'île de Groix. Thèse de 3ème cycle, Université de Rennes, 145 pp.
- Quinquis, H. & Choukroune, P. (1981). Les schistes bleus de l'île de Groix dans la chaîne hercynienne: implications cinématiques. *Bulletin de la Société Géologique de France (7)* **XXIII**, 409–418.
- Rüpke, L. H., Morgan, J. P., Hort, M. & Connolly, J. A. D. (2004). Serpentine and the subduction zone water cycle. *Earth and Planetary Science Letters* **223**, 17–34.
- Ryan, J., Morris, J., Bebout, G. & Leeman, B. (1996). Describing chemical fluxes in subduction zones: insights from 'depth-profiling' studies of arc and forearc rocks. In: Bebout, G., Scholl, D. W., Kirby, S. H. & Platt, J. P. (eds) *Subduction: Top to Bottom. Geophysical Monograph, American Geophysical Union* **96**, 263–268.
- Scambelluri, M. & Philippot, P. (2001). Deep fluids in subduction zones. *Lithos* **55**, 213–227.
- Schmidt, M. W. & Poli, S. (1998). Experimentally based water budgets for dehydrating slabs and consequences for arc magma generation. *Earth and Planetary Science Letters* **163**, 361–379.
- Schmidt, S. Th., El Korh, A. & Ulianov, A. (2008). Recycling of trace and rare earth elements in HP/LT assemblages of metabasites, Ile de Groix, France. Goldschmidt 2008 Abstracts, Vancouver. *Geochimica et Cosmochimica Acta* **72**(12), Supplement 1, A836.
- Schulz, B., Triboulet, C., Audren, C., Pfeifer, H.-R. & Gilg, A. (2001). Two-stage prograde and retrograde Variscan metamorphism of glaucophane-eclogites, blueschists and greenschists from the Ile de Groix (Brittany, France). *International Journal of Earth Sciences* **90**, 871–889.
- Seno, T. & Gonzalez, G. (1987). Faulting caused by earthquakes beneath the outer slope of the Japan trench. *Journal of Physics of the Earth* **35**, 381–407.
- Shatsky, V. S., Kozmenko, O. A. & Sobolev, N. V. (1990). Behaviour of rare earth elements during high-pressure metamorphism. *Lithos* **25**, 219–226.
- Sorensen, S. S., Grossman, J. N. & Perfit, M. R. (1997). Phengite-hosted LILE enrichment in eclogite and related rocks: implications for fluid-mediated mass transfer in subduction zones and arc magma genesis. *Journal of Petrology* **38**, 3–34.
- Spandler, C. J., Hermann, J., Arculus, R. J. & Mavrogenes, J. A. (2003). Redistribution of trace elements during prograde metamorphism from lawsonite blueschist to eclogite facies; implications for deep subduction-zone processes. *Contributions to Mineralogy and Petrology* **146**, 205–222.

- Spandler, C. J., Hermann, J., Arculus, R. J. & Mavrogenes, J. A. (2004). Geochemical heterogeneity and element mobility in deeply subducted oceanic crust; insights from high-pressure basic rocks from New Caledonia. *Chemical Geology* **206**, 21–42.
- Sun, S. S. & McDonough, W. F. (1989). Chemical and isotopic systematics of oceanic basalts: implications for mantle composition and processes. In: Saunders, A. D. & Norry, M. J. (eds) *Magmatism in the Ocean Basins*. Geological Society, London, *Special Publications* **42**, 313–345.
- Tatsumi, Y., Hamilton, D. L. & Nesbitt, R. W. (1986). Chemical characteristics of fluid phases released from a subducted lithosphere and origin of arc magma: evidence from high-pressure experiments and natural rocks. *Journal of Volcanology and Geothermal Research* **29**, 293–309.
- Taylor, S. R. & McLennan, S. M. (1981). The composition and evolution of the continental crust: rare earth element evidence from sedimentary rocks. *Philosophical Transactions of the Royal Society of London, Series A* **301**, 381–399.
- Triboulet, C. (1974). Les glaucophanites et roches associées de l'île de Groix (Morbihan, France): étude minéralogique et pétrogénétique. *Contributions to Mineralogy and Petrology* **45**, 65–90.
- Tribuzio, R., Messiga, B., Vannucci, R. & Bottazzi, P. (1996). Rare earth element redistribution during high-pressure–low-temperature metamorphism in ophiolitic Fe-gabbros (Liguria, northwestern Italy); implications for light REE mobility in subduction zones. *Geology* **24**, 711–714.
- Usui, T., Kobayashi, K., Nakamura, E. & Helmstaedt, H. (2007). Trace element fractionation in deep subduction zones inferred from a lawsonite-eclogite xenolith from the Colorado Plateau. *Chemical Geology* **239**, 336–351.
- You, C. F., Castillo, P. R., Gieskes, J. M., Chan, L. H. & Spivack, A. J. (1996). Trace element behavior in hydrothermal experiments: Implications for fluid processes at shallow depths in subduction zones. *Earth and Planetary Science Letters* **140**, 41–52.
- Zack, T. & John, T. (2007). An evaluation of reactive fluid flow and trace element mobility in subducting slabs. *Chemical Geology* **239**, 199–216.
- Zack, T., Rivers, T. & Foley, S. F. (2001). Cs–Rb–Ba systematics in phengite and amphibole: an assessment of fluid mobility at 2.0 GPa in eclogites from Trescolmen, Central Alps. *Contributions to Mineralogy and Petrology* **140**, 651–669.
- Zack, T., Foley, S. F. & Rivers, T. (2002). Equilibrium and disequilibrium trace element partitioning in hydrous eclogites (Trescolmen, Central Alps). *Journal of Petrology* **43**, 1947–1974.